The Thesis Committee for Anoosha Izadi
Certifies that this is the approved version of the following thesis:

Quantitative Characterization of Microstructure of Asphalt Mixtures to Evaluate Fatigue Crack Growth

APPROVED BY
SUPERVISING COMMITTEE:

Supervisor:

Amit Bhasin

Andre Smit

Quantitative Characterization of Microstructure of Asphalt Mixtures to Evaluate Fatigue Crack Growth

by

Anoosha Izadi, B.S.

Thesis

Presented to the Faculty of the Graduate School of

The University of Texas at Austin

in Partial Fulfillment

of the Requirements

for the Degree of

Master of Science in Engineering

The University of Texas at Austin

May 2012

Acknowledgements

I am grateful to my advisor, Dr. Bhasin, for his encouragement and support throughout my research. His vast knowledge of the subject and his patience in guiding me truly helped me in all the time of research and writing of this thesis.

I also would like to thank Dr. Smit for reading a draft of my thesis and providing constructive feedback.

Abstract

Quantitative Characterization of Microstructure of Asphalt Mixtures to Evaluate Fatigue Crack Growth

Anoosha Izadi, M.S.E

The University of Texas at Austin, 2012

Supervisor: Amit Bhasin

Studies show that the microstructure of the fine aggregate matrix has a significant influence on the mechanical properties and evolution of damage in an asphalt mixture. However, very little work has been done to quantitatively characterize the microstructure of the asphalt binder within the fine aggregate matrix of asphalt mixtures. The first objective of this study was to quantitatively characterize the three dimensional microstructure of the asphalt binder within the fine aggregate matrix (FAM) of an asphalt mixture and compare the influence of binder content, coarse aggregate gradation, and fine aggregate gradation on this microstructure. Studies indicate that gradation of the fine aggregate has the most influence of the degree of anisotropy whereas gradation of the coarse aggregate has the most influence on the direction anisotropy of the asphalt mastic within the fine aggregate matrix. Addition of asphalt binder or adjustments to the fine

aggregate gradation also resulted in a more uniform distribution of the asphalt mastic within the fine aggregate matrix.

The second objective of this study was to compare the internal microstructure of the mortar within a full-scale asphalt mixture to the internal microstructure of the FAM specimen and also conduct a limited evaluation of the influence of mixture properties and methods of compaction on the engineering properties of the FAM specimens. Fatigue cracking is a significant form of pavement distress in flexible pavements. The properties of the sand-asphalt mortars or FAM can be used to characterize the evolution of fatigue crack growth and self-healing in full-scale asphalt mixtures. The results from this study, although limited in number, indicate that in most cases the SGC (Superpave Gyratory Compactor) compacted FAM specimen had a microstructure that most closely resembled the microstructure of the mortar within a full-scale asphalt mixture. Another finding from this study was that, at a given level of damage, the healing characteristic of the three different types of FAM mixes evaluated was not significantly different. This indicates that the healing rate is mostly dictated by the type of binder and not significantly influenced by the gradation or binder content, as long as the volumetric distribution of the mastic was the same.

Table of Contents

List of Tables

List of Figures

Chapter 1. Introduction

1.1 Project Background

Fatigue cracking is a significant form of distress in flexible pavements. The most common method to quantify the resistance of asphalt mixtures to fatigue cracking and other distress mechanisms is to perform mechanical tests under controlled laboratory conditions on mixture specimens. The advantage of this approach is that candidate mixtures can be ranked based on their performance using a simple laboratory test. Another advantage of this approach is that it takes into account the combined affect of material and mixture properties on mixture performance. However, there are three major limitations to this approach. First, it does not provide any information that can be used to explain why certain mixtures perform better than others. This in turn limits the ability of the engineer to take cost effective remedial actions to improve the performance of poor performing mixtures. Second, the evolution of damage from some of the traditional laboratory performance tests is dependent on the test conditions (e.g. specimen geometry or mode of loading) and cannot be extrapolated to field conditions. Finally, the results obtained by conducting tests on full-scale asphalt mixtures often have a very high variability.

To alleviate some of these shortcomings, several research studies have been undertaken to investigate the properties and performance of asphalt mixtures at multiple scaling dimensions. For example, constituent materials (e.g. binder, aggregate, and fines) are evaluated in order to identify their contribution to mixture properties and damage evolution. Properties of mastics (fines mixed with asphalt binder) are evaluated to

understand filler-binder interactions. Evaluation of sand-asphalt mortars or FAM provides information on the evolution of damage in this phase, role of fines to arrest crack growth, and moisture damage. Evaluation of full-scale asphalt mixtures helps identify the role of coarse aggregate properties and mixture microstructure in resistance of the mixture to damage.

In order to better understand the mechanical properties of asphalt mixture, the microstructure of the sand-asphalt is first investigated in this research and the influence of mixture design characteristics (e.g. binder content and gradation) are examined on the microstructure of the full-scale and FAM mixes. Then, the influence of mixture design characteristics (e.g. binder content and gradation) and the methods of compaction are examined on the engineering properties of the FAM mixes.

There is significant evidence in the literature that demonstrates that the microstructure of the sand-asphalt dictates the mechanical properties and evolution of damage within the full-scale asphalt mixture. However, in the context of asphalt mixtures the term microstructure is not well defined. There have been very few attempts to derive a quantitative metric for the microstructure of asphalt mixtures. Developing a quantitative method to describe the three dimensional microstructure of asphalt mixtures has several potential applications and advantages. For example, a quantitative measure of the microstructure of asphalt mixtures can be used to (i) characterize the average three dimensional geometry of the asphalt binder matrix that holds the aggregates together, (ii) estimate the level of anisotropy of different components within the asphalt mixtures, (iii) understand the relationship between shape characteristics of the asphalt binder matrix and performance related aspects such as development of confining stresses, and (iv) estimate the influence of aggregate shape and binder content on the shape of the asphalt binder matrix.

The Dynamic Mechanical Analysis (DMA) is typically used to characterize the performance and engineering properties of the fine aggregate matrix or the sand-asphalt mortar, hereafter referred to as fine aggregate matrix (FAM) for brevity. Distresses such as fatigue crack growth are concentrated in the sand-asphalt mortar or FAM phase of the mixture (Kim and Little, 2005). Therefore the DMA of FAM specimens provides a magnified view of the fatigue cracking characteristics of the mixtures being investigated. This approach can be used to (i) evaluate the response and rank the performance of different material combinations, (ii) evaluate the efficacy of using additives such as warm mix agents, liquid anti-strip agents or hydrated lime, and (iii) provide required mechanical properties as an input for computational modeling of full-scale asphalt mixtures (Kim et al., 2003; Kim et al., 2004; Kim and Little, 2005; Masad et al., 2006; Branco et al., 2008; Caro et al., 2008). For each of the aforementioned applications, it is important that the FAM represent the design and internal structure of the sand-asphalt mortar phase from the full-scale asphalt mixture as closely as possible. A short review of some of the methods to design and fabricate the FAM specimens is presented below.

Kim et al., (2003) reported the use of sand-asphalt mixture to evaluate the influence of fillers such as hydrated lime and limestone fines on the rheological properties of the asphalt binder and the mix. They used different filler to asphalt binder ratios and Ottawa sand to produce the sand-asphalt mixtures. They measured the linear viscoelastic properties of these mixtures and subjected the test specimens to a time sweep or fatigue test using a Dynamic Shear Rheometer (DSR). The results from these tests were used with continuum mechanics to quantify the influence of different fillers on the performance of different asphalt binders. Kim et al. used fine aggregates as a carrier to fabricate mortar specimens with different filler to binder ratios. In studies that followed

Kim et al., researchers replicated the mortar (in terms of the material and gradation) from a specific full-scale asphalt mixture in lieu of using a standard fine aggregate (such as Ottawa sand) to fabricate FAM specimens. The two main advantages of this approach are:

1. The mechanical properties and physiochemical interactions between the aggregate and binder are replicated in the FAM specimen. Consequently, the damage evolution of the mortar specimens can be measured and used as a material screening tool for the design of optimal performing mixtures.
2. The mechanical properties and the damage evolution in the FAM specimens can be measured and used as an input for computational models to determine the response of full-scale asphalt mixtures.

For example, Zollinger, (2005) selected the fine aggregates and gradation from eight different asphalt mixtures with known field performance. The gradation of the fine aggregates (in this case defined as aggregates passing 1.18 mm sieve) in the FAM followed the same proportions as that of the selected full-scale asphalt mixture and the binder content was selected such that the volume of filler (fines passing number 200 sieve) was 10 percent the volume of the binder. Zollinger, (2005) used a Superpave Gyratory Compactor (SGC) to compact a six-inch diameter and approximately three-inch tall mortar specimen with a target air void content of eleven percent. Approximately twenty test specimen, two inch in height and 1/2" in diameter, were obtained by sawing and coring each SGC compacted specimen. The fatigue cracking life of the FAM specimens for the eight different asphalt mixtures were tested with and without moisture conditioning. Results were shown to correlate well with the observed field performance of these mixtures. Caro et al., (2008) also used a similar approach to design FAM specimens to evaluate the moisture sensitivity of five different asphalt mixtures and the

contribution of hydrated lime to improve the moisture damage resistance of certain mixtures. Masad et al., (2006) and Branco et al., (2008) used a similar approach with a slight modification to characterize the fatigue cracking life under different modes of loading for FAM specimens. Instead of using a constant binder to filler volume ratio, Branco et al., (2008) adjusted the binder content to reflect the binder content within the mortar phase of the full-scale asphalt mixture. In other words, the mass percent of the binder in the FAM was the same as the percentage of binder by mass of fine aggregates in the full-scale asphalt mixture.

In summary, several different approaches have been suggested to design the FAM based on the mixture design of a full-scale asphalt mixture. However, there is no evidence to support the premise that the microstructure of the sand-asphalt mixtures fabricated in the laboratory is similar to the microstructure of the sand asphalt portion of a full-scale asphalt mixture. Different researchers have used different approaches to design the FAM mixtures based on different assumptions. This is a significant knowledge gap that must be addressed to allow proper design of FAM mixtures in order to have meaningful and accurate relationship to full-scale mixture properties and performance modeling.

1.2 OBJECTIVES

This study has four main objectives. The first objective of this study is to address the first and most critical step in the pursuit of relating mixture microstructure to its properties, i.e. to establish a quantitative method to characterize the three dimensional microstructure of the asphalt binder in an asphalt mixture. This was achieved by accomplishing the following key steps.

- Asphalt mixture specimens with different aggregate gradations and binder contents were fabricated in the laboratory.
- Representative volumes of these asphalt specimens where then scanned using very high resolution three-dimensional X-ray computed tomography (X-Ray CT). Note that unlike previous studies, the focus of this study was to evaluate the three dimensional microstructure of asphalt binder or mastic in a mixture. Consequently, smaller representative portions of the full-scale asphalt mixture specimen were scanned using very high resolution X-ray CT instead of lower resolution scans of full-scale asphalt mixture specimens.
- The scanned gray scale X-ray CT images were processed to eliminate noise and determine the gray scale thresholds that separate the three phases, asphalt binder, aggregate and air voids based on measured volumetric properties.
- The star length distribution (SLD) parameter was used to characterize the shape of the asphalt binder matrix in the mixture. Change in aggregate gradation and binder content was used to describe the change in microstructure of the asphalt mixtures via the SLD parameter.
- Parameters based on the SLD such as the fabric tensor were used to estimate the level of anisotropy in the mixture. Variability in the SLD was used to quantify the expected variability in the mixture properties along specific directions.

The other three objectives of this study are to: (i) compare the internal microstructure of the mortar from a full-scale asphalt mixture to the internal microstructure of the FAM specimen for different mix designs, (ii) to evaluate whether the method of compaction used to fabricate FAM specimens has any influence on its mechanical properties, and (iii) to evaluate the influence of mixture design characteristics

such as gradation and binder content on the performance of the FAM specimens. These objectives were achieved by accomplishing the following key steps.

- Asphalt mixture specimens with different aggregate gradations and binder contents were fabricated in the laboratory using the Superpave Gyratory Compactor. FAM specimens replicating the designs from the full-scale asphalt mixtures were fabricated using three different compaction methods.
- Representative volumes of the FAM specimens were also scanned using very high-resolution three-dimensional X-ray computed tomography (X-Ray CT). The objective of this task was to compare the three-dimensional microstructure of the mortar from a full-scale asphalt mixture to the microstructure of a FAM specimen representing a comparable mix design. The star length distribution (SLD) was selected as a metric to compare the internal microstructure of the FAM specimens to the internal microstructure of the mortar from the full-scale asphalt mixture.
- Mechanical properties of the FAM specimens, including stiffness, fatigue cracking resistance, and propensity to heal were measured using the DMA. These properties were compared for FAM specimens with similar mix designs compacted using different methods as well as FAM specimens with different mix designs.

1.3 THESIS STRUCTURE

This thesis consists of five chapters. The first chapter is on the project background and objectives of this study. The second chapter summarizes the findings from a detailed literature review on three aspects, (i) importance of internal microstructure on the performance of asphalt mixtures and methods used to determine the internal microstructure, (ii) methods to pre-process and enhance images, and (iii) metrics to

quantify internal microstructure of composite materials and relationship of these metrics to mechanical properties of the composite. This chapter also presents the relevant background on the use of DMA to determine stiffness, fatigue cracking resistance and healing characteristics of the mortar specimens. The third chapter presents details of the methodology used to fabricate specimens, to collect and process the image data. Chapter four presents the experiment design and the detailed analysis of results and Chapter five presents a discussion of findings and conclusions from this study.

Chapter 2. Literature Review

This chapter can be divided into four main parts, which are very useful in understanding the goals of this research:

- Internal structure of asphalt mixtures
- Image processing
- Image analysis
- Characterization of mechanical properties of mortar specimens

2.1 Internal Structure of Asphalt Mixtures and Other Composites

The term internal structure of an asphalt concrete mixture refers to the content and spatial distribution of asphalt, aggregates and air-voids (Masad et al., 1999a). The internal structure of the mixture is dictated by the proportions and properties of its constituent materials and method of compaction. It is well recognized that the internal structure of an asphalt mixture plays a significant role in influencing the mechanical properties and the resistance of the mixture to major distresses including rutting, fatigue cracking, thermal cracking and low temperature cracking. Most mixture design methods recognize the importance of internal microstructure by imposing requirements for aggregate size, gradation, shape, density during compaction, and volumetrics (Masad and Button, 2004).

In the past decade several research studies have used more direct methods, such as imaging techniques, to characterize the internal microstructure of asphalt mixtures. Three basic steps are typically required to characterize the internal microstructure using this direct approach. The first step is to acquire two-dimensional (2D) or three-dimensional

images (3D) of the composite. Digital cameras can be used to acquire 2D image of a cross-section or a series of images for cross-sections that are obtained by physically dissecting the specimen into several slices. An alternative approach is to use non-destructive techniques such as 3D X-ray tomography that provide a stack of 2D images for a volume of interest at varying resolutions. The second step is to process the image to eliminate noise and identify regions of interest (e.g. aggregate, air void). Section 2.2 presents more details on image processing. The last step is to identify metrics that can be used to quantify the characteristic of interest (e.g. size of voids, orientation of aggregates). Section 2.3 presents more details on image analysis. Image analysis of internal microstructure has been applied in three broad areas discussed below.

First, image analysis has been used to investigate the influence of compaction on the internal microstructure of asphalt mixtures. For example, Masad et al., (1999a) used X-ray tomography to establish the relationship of aggregate orientation, aggregate gradation, and air void distribution to the compaction effort. The study included specimens compacted in the laboratory using the Superpave gyratory compactor (SGC) with different number of gyrations as well as field cores. The orientation of an aggregate was measured as the angle between its major axis and a horizontal line on the scanned image. Anisotropy in aggregate orientation was quantified based on the distribution of the aggregate orientations. Aggregate and air void size distributions were obtained by measuring the area on the two- dimensional sectional images obtained from X-ray tomography. The bias due to the use of two-dimensional sectional images to obtain aggregate size distribution was corrected using Monte-Carlo simulations. Due to limitations in the resolution of images obtained from the X-ray tomography, comparisons of aggregate size distribution and orientations to compaction effort were limited to coarse aggregates. Masad et al., (1999a) concluded that specimens compacted using a low

number of gyrations resulted in a uniform void distribution throughout the specimen height. On the other hand, at higher number of gyrations the middle part of the specimen had fewer air voids. In another study, Masad et al., (1999b) quantified the internal structure of the asphalt mixtures in terms of the aggregate orientation, points of contact and distribution of air voids. These characteristics were compared for mixtures compacted using the SGC and the linear kneading compactor (LKC). The erosion operation technique, which is a noise reduction operation in image processing, was used to determine the number of contact points. Masad et al., (1999b) concluded that the aggregates in the SGC have preferred orientation toward horizontal direction while aggregates in the LKC had a more random distribution. They also concluded that the aggregates in LKC specimens had more point-to-point contacts as compared to the SGC specimens. They suggested that higher aggregate contact points in the LKC specimens resulted in higher shear strength in specimens compacted using the LKC due to inter particle contact. Finally, they concluded that air voids were concentrated at the top and the bottom portions of the SGC compacted specimens and at the bottom of the LKC specimens. Hunter et al., (2004) also investigated the change in internal microstructure of asphalt mixtures as influenced by the method of compaction. Radial and circumferential particle alignment and area of particles in fixed radial quadrants were used to examine variations in aggregate orientation and distribution within the asphalt mixture. They concluded that depending on the method of compaction, mixtures with similar bulk volumetric properties demonstrated different levels of preferred circumferential and radial orientations.

Second, image analysis has been used to investigate the influence of internal microstructure on the engineering properties and performance of asphalt mixtures. For example, Yue et al., (1995) used image analysis to quantify anisotropy in an asphalt

mixture based on the orientation of aggregates. Directional distribution of aggregates was quantified based on the ratio of average area per aggregate in horizontal sections to the average area per aggregate in vertical sections. Wang et al., (2001) demonstrated that field cores with similar volumetric properties exhibited different internal microstructure that correlated better with their observed field performance. Void content, void distribution, and mean solid path were measured on sectional images obtained using X-ray tomography. An interpolation algorithm was developed and used to create intermediate sectional images in order to compensate for the lower vertical resolution as compared to the horizontal resolution for the images. Masad et al., (2002) and Tashman et al., (2005) used two-dimensional image analysis to quantify aggregate distribution on cut sections of asphalt mixtures to determine the level of anisotropy. They then used this as one of the model parameters to improve the predictions of viscoplastic deformation in asphalt concrete mixtures. Arambula et al., (2007) demonstrate that the aggregate gradation and compaction effort influence the size and distribution of air voids within an asphalt mixture. The size and distribution of air voids were shown to have a strong influence on the rate of moisture damage in the asphalt mixtures. The relationship of internal microstructure and mechanical properties has also been long recognized and used for materials other than asphalt mixtures. For example, according to Ryan and Ketcham, (2002) the relationship between the trabecular bone morphology and skeletal loads was first investigated in 1867. Cowin, (1985) investigated the relationship between the stiffness tensor of a trabecular bone to its "fabric". He introduced the term fabric as a measure of the local anisotropy of a material's microstructure. Duxson et al., (2005) demonstrated a correlation between mechanical strength and Young's modulus of geopolymers and their microstructure .

Finally, image analysis has been used to derive the internal microstructure of asphalt mixtures that serves as the required geometry input for computational modeling. For example, Wang et al., (2007) describe methods to extract three-dimensional geometric features of aggregates from X-ray CT images. You et al., (2009) developed a two-dimensional and three dimensional discrete element models to predict the dynamic modulus of asphalt concrete mixtures. The required geometry for these models was obtained using X-ray CT imaging. The authors reduced the three dimensional images of real asphalt mixtures into three different components, coarse aggregates, fine aggregate-binder mortar, and air voids. Zelelew et al., (2008) developed volumetric based global minima thresholding algorithms to process asphalt concrete X-ray CT images. This technique was used to distinguish between air, mortar and coarse aggregates within a full-scale asphalt mixture based on the volumetric properties of the mixture thus allowing for a more accurate and calibrated geometric representation of these components that can be used in subsequent computational modeling.

Tutumluer et al., (2008) used imaging methods to extract the geometry of aggregates used in granular materials for discrete element modeling (DEM). They used DEM to demonstrate the influence of aggregate angularity and surface texture on the shear properties of granular base materials.

While the previous studies have recognized the importance of the distribution or structure of the binder matrix itself, very little work has been done to quantify this distribution. In 1930s Hveem introduced the concept of film thickness to design asphalt mixtures. The methods used to calculate the film thickness (that would result in optimal performance of the mixture) were approximate and relied on several unrealistic assumptions. More recently, Elseifi et al., (2008) used reflective light microscopy and scanning electron microscopy to demonstrate that a uniform film coating the aggregates

did not actually exist in the asphalt mix. They demonstrated that film thickness varied greatly within the same specimen and around the same aggregate. They also reported that mineral fillers and finer aggregates were embedded in the asphalt binder such that the behavior of the binder itself may not be as critical as the behavior of the mastic.

In summary, distribution of air voids, solid path between air voids, orientation and points of contacts between coarse aggregates were typically used as the metrics to describe the internal microstructure of asphalt mixtures. In most cases, these metrics were obtained using individual 2D sectional images of a mixture specimen and do not directly characterize the binder matrix. The objective of this research was to identify a method and concomitant parameter by which to quantify the three dimensional internal microstructure of asphalt binder or mastic based on the collective analysis of all sectional planes for a mixture specimen obtained using x-ray tomography. Although the methodology discussed in this study is applied to characterize the internal microstructure of the asphalt mastic, it can also be used to characterize the three-dimensional microstructure of any component in the mixture (e.g. air voids, aggregates, mortar).

2.2 IMAGE PROCESSING

Digital images acquired from X-ray CT scanning or any other method are typically in gray scale and contain some amount of noise. The acquired images must be processed prior to using them for any kind of analysis. This section presents a short review of some of the methods that were investigated and used to process the images used in this study. Image processing can be broken down into three major steps:

1. Contrast enhancement
2. Noise reduction
3. Thresholding

Each one of these key steps is briefly discussed in the subsections below.

2.2.1 Contrast Enhancement

Although contrast enhancement is not critical for computational analysis of images, it is usually performed to improve visibility of the image and allows the user to clearly differentiate the components in an image. There are two techniques available to perform contrast enhancement,

- Histogram equalization and
- Best fit equalization.

Histogram equalization is the most common technique used for contrast enhancement. Histogram equalization is achieved by transforming a small range of values from an intensity image, or the values in the color map of an indexed image, so that the histogram of the output image approximately matches a specified histogram with a broader range of values. For example, Figure 2.1 shows application of histogram equalization technique on an image of an asphalt concrete mixture. The original image in Figure 2.1 has intensity values ranging from 0-165, while the image after histogram equalization spans the full range of available intensity values, i.e. 0-256. The best-fit equalization method maps the intensity values from the original gray scale image to new values such that 1% (can be varied) of data is saturated at low and high intensities of the original image. This increases the contrast of the output image. Figure 2.2 illustrates the typical results from using the best-fit equalization on an image of an asphalt concrete mixture.

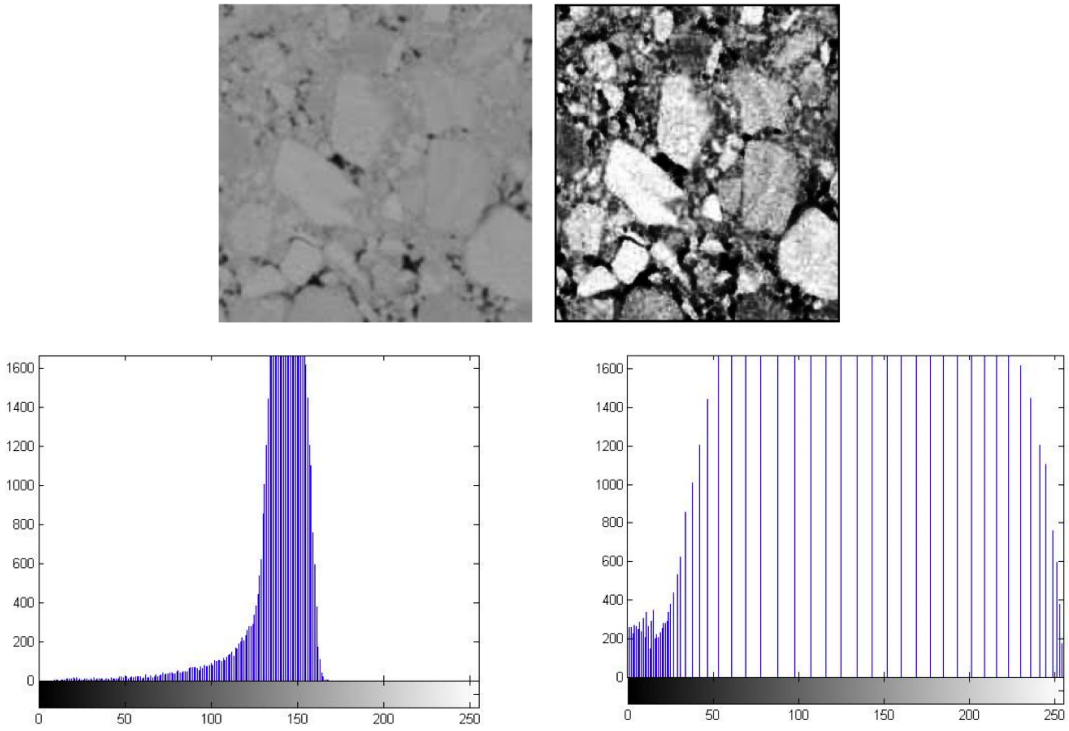

Figure 2.1. Contrast Enhancement Using Histogram Equalization. (Left: Before Enhancement, Right: After Enhancement)

2.2.2 Noise Reduction

This is perhaps the most important step in image processing. Noise is defined as random, usually unwanted, variation in brightness or color information of an image. This randomness leads to erroneous interpretation of image data and hence needs to be addressed before any analysis is carried out. In the case of X-ray CT images, the most

common source of noise is counting statistics in the image detector due to a small number of incident particles such as electron or photon (Russ, 2007). Other common sources include inadequate or non-uniform illumination, undesirable viewpoint, issues with alignment, sensor quality, as well as image digitizing and pre-processing.

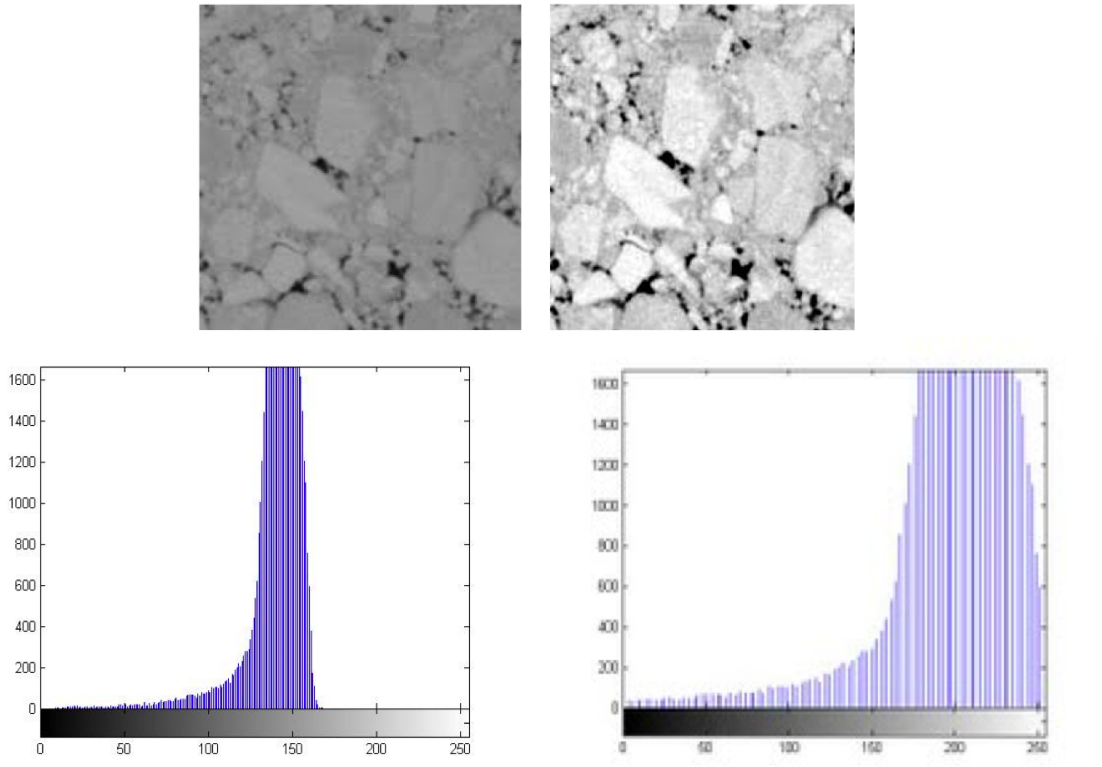

Figure 2.2. Contrast Enhancement Using Best Fit Equalization. (Left: Before Enhancement, Right: After Enhancement)

In general, the common types of noise associated with images are random (or Gaussian) noise, shot (or salt pepper) noise, film grain, and non-isotropic noise. Random noise is the most common form of noise in images of asphalt concrete mixtures obtained using X-ray CT scans. Images from X-ray CT scanning can also have artifacts due to beam hardening, a process by which X-rays with lower intensity are attenuated while rays with higher intensity continue to traverse through the medium.

There are three common methods that can be used to reduce random noise. There are several different sub-methods under for each one of these three methods:

- Neighborhood averaging,
- Median neighborhood ranking, and
- Mode neighborhood tanking.

The underlying assumption to apply these methods is that pixels in the image are much smaller than any of the important details. Another assumption is that the structure represented by a pixel and its neighborhood is very similar. The basic principle for the three methods is the same, i.e. for a given pixel, its original intensity value is replaced by a new value obtained by performing a mathematical operation on the intensity values of the neighboring pixels. In case of the neighborhood averaging method, the intensity of a pixel is replaced by the mean intensity of the pixels within a defined neighborhood of the subject pixel. Similarly, in the case of median or mode ranking methods, the pixel intensity is replaced by the median or mode of intensity of pixels within a defined neighborhood of the subject pixel. An important variable in applying these techniques is the size of the neighborhood that is used to compute the intensity of a pixel based on its mean, median or mode.

As stated above, neighborhood averaging replaces the original pixel value by the average all pixel values around its neighborhood. The advantage of this technique is that

it is very effective in reducing shot noise. However, one of the limitations of this method is that it blurs the edges of different entities within the image. This in turn reduces the accuracy of edge detection that may be performed on the images later. Neighborhood averaging also results in boundary displacement and contrast reduction. Other variations of neighborhood averaging such as weighted average filter, and the "Olympic" filter may be used to offset these limitations to some extent. Figure 2.3 presents an original and filtered image by performing neighborhood averaging using a 3x3 matrix and a 9x9 matrix. Notice that the use of a larger matrix size (averaging across a larger neighborhood) results in reduced noise but greater distortion in the image.

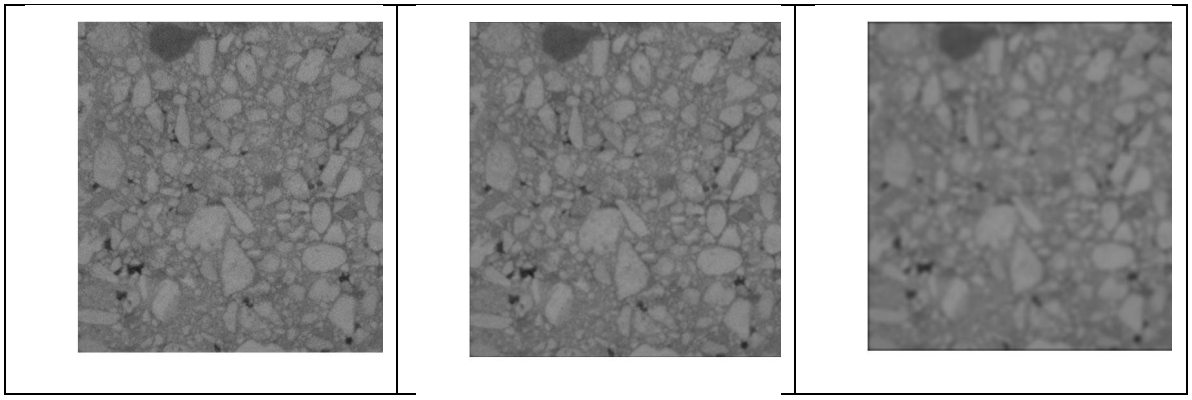

Figure 2.3. Use of Neighborhood Averaging to Reduce Noise. (Left: Before Filtering, Middle: Neighborhood Averaging with 3x3 Matrix, Right: Neighborhood Averaging with 9x9 Matrix)

In the median neighborhood ranking method, the pixel value is replaced by the median of neighborhood pixel values. This involves ranking of pixel intensity values within a neighborhood and assigning the median value to the central pixel. This technique overcomes most of the limitations of neighborhood averaging, especially related to blurring of edges. Also, as the name suggests, median neighborhood ranking is not as

sensitive to outliers or extreme data points in the neighborhood as compared to the neighborhood averaging. It is useful in reducing shot noise and it does not result in shifting of boundaries or reduced brightness difference across steps. The main limitation of this technique is that it erases fine lines and rounds corners. However, if the objective of image analysis is to detect features and separate different entities within the image, as in the case of analysis of the internal structure of asphalt mixtures, the median neighborhood ranking method would be preferred to the neighborhood averaging method. Figure 2.4 presents an original and filtered image by performing median neighborhood ranking.

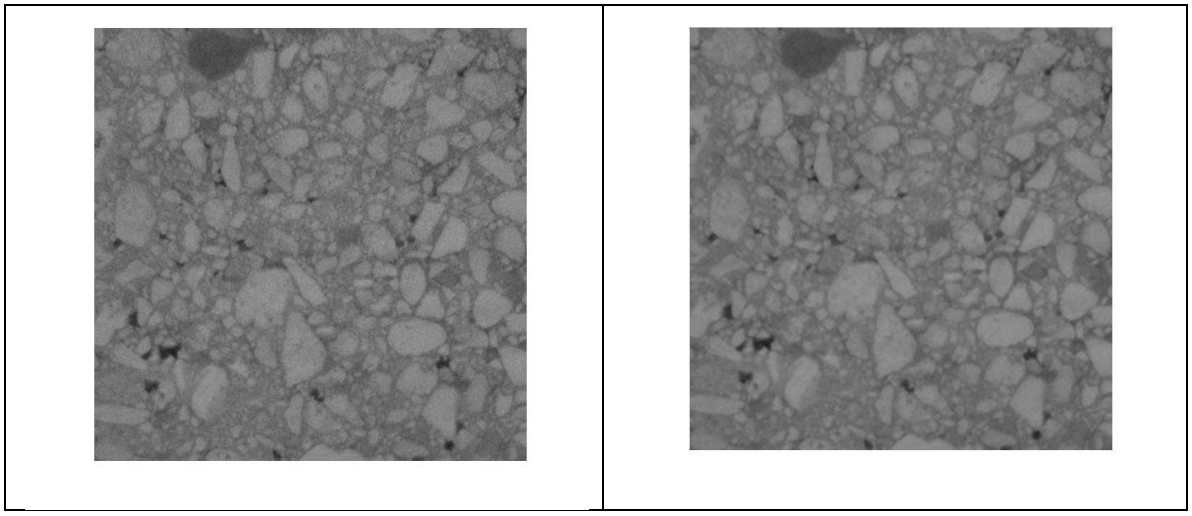

Figure 2.4. Use of Median Neighborhood Ranking with 3x3 Matrix to Reduce Noise.
(Left: Before Filtering, Right: Median Neighborhood Ranking)

The mode neighborhood ranking filter replaces the value of each pixel with the mode of the pixel values in its neighborhood. Although this filter has many advantages

over the previous two filters, a serious limitation is that it can only be used with a small neighborhood. Therefore, this technique was not considered appropriate for this study.

2.2.3 Thresholding

An asphalt mixture is made up of three components, air, asphalt binder (or mastic = binder + fines), and aggregates. Each of these components has a significantly different density from the other. In order to characterize the internal structure of the asphalt mixture it is of interest to clearly differentiate these three components in the image. X-ray CT images of asphalt mixture specimens are created by measuring the attenuation of the X-rays traveling through the specimen. The amount of attenuation is proportional to the density of the material. Consequently, a high intensity or bright pixel indicates a high-density material (such as an aggregate) and a dark pixel indicates a low-density material or phase (such as air void). However, due to inherent variability in the densities of these materials and finite resolution of the imaging process, the X-ray CT images do not contain three pixel intensity values corresponding to each of the three components. Instead, the CT images are gray scale images with pixel values ranging from 0 to 255. Thresholding is the most critical step that allows the user to reduce these gray scale images to binary or trinary images with just two or three pixel values to represent any two or all three components of interest. The following is a brief review and background of approaches for thresholding a gray scale image to a binary image that clearly distinguishes between the two components of a composite using two different pixel intensity values. The same concepts can be extended to obtain a trinary image that uses three pixel intensity values to represent three components in the composite.

Thresholding can be performed either automatically based on standard algorithms or manually based on specific algorithms defined by the user. The automatic approach

works on the principle that there are only two components present in the image and the threshold level is defined as the pixel value that separates these two components. Figure 2.5 shows histogram for such a composite. For this example, a typical automated thresholding algorithm will tend to select the pixel value that produces the smallest value between the two peaks. For Figure 2.5 this threshold level value is approximately 125. Figure 2.6 illustrates the results from applying the automatic threshold algorithm on an image of an asphalt concrete specimen. The threshold level selected by imaging processing software to differentiate aggregates from air, asphalt binder and possibly fine aggregates was 129.5. The main advantage of this method is that the results are consistent and no judgment is involved in the approach. However, this automated approach can only be applied when there are only two easily distinguishable components present in the image. There are several instances, in which such an automated algorithm can very easily produce misleading results.

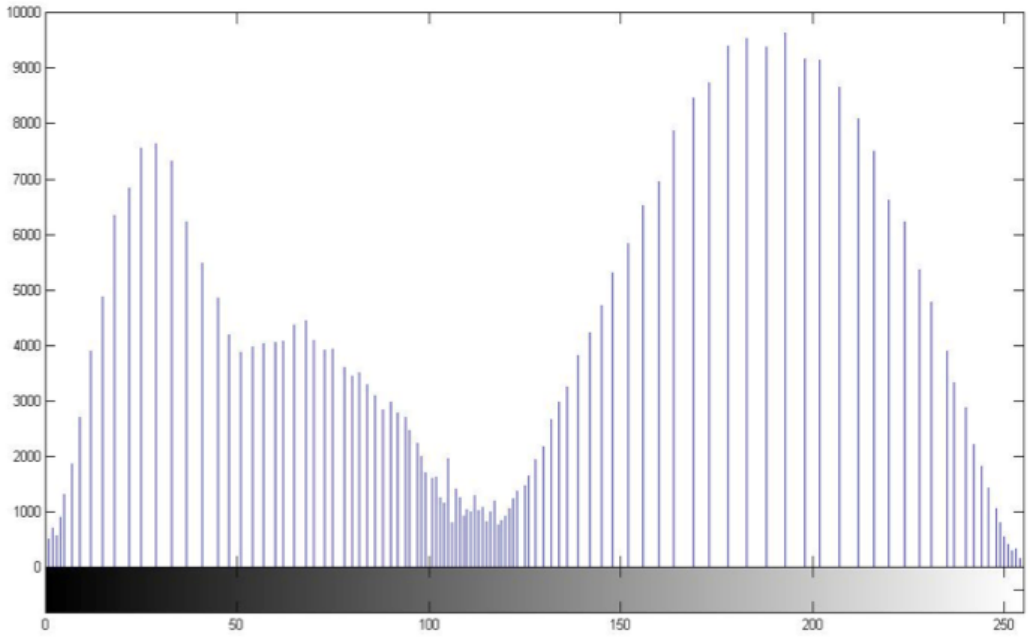

Figure 2.5. Histogram of a Composite With Two Components.

There are two ways to mitigate the limitations associated with the automatic approach. The first is to manually select a threshold based on the users judgment. This approach can be highly subjective and result in inconsistent interpretation of results from image analysis depending on the user. Figure 2.7 shows the results from application of manual thresholding on the same image as in Figure 2.6 with threshold level 73 to differentiate aggregates from air, asphalt binder and possibly fines. The second and more robust approach is to iteratively select different thresholds until the measured area fraction (or volume fraction) of each of the two components from the image (or a stack of images representing a three dimensional structure) matches previously known or directly measured area fraction (or volume fraction).

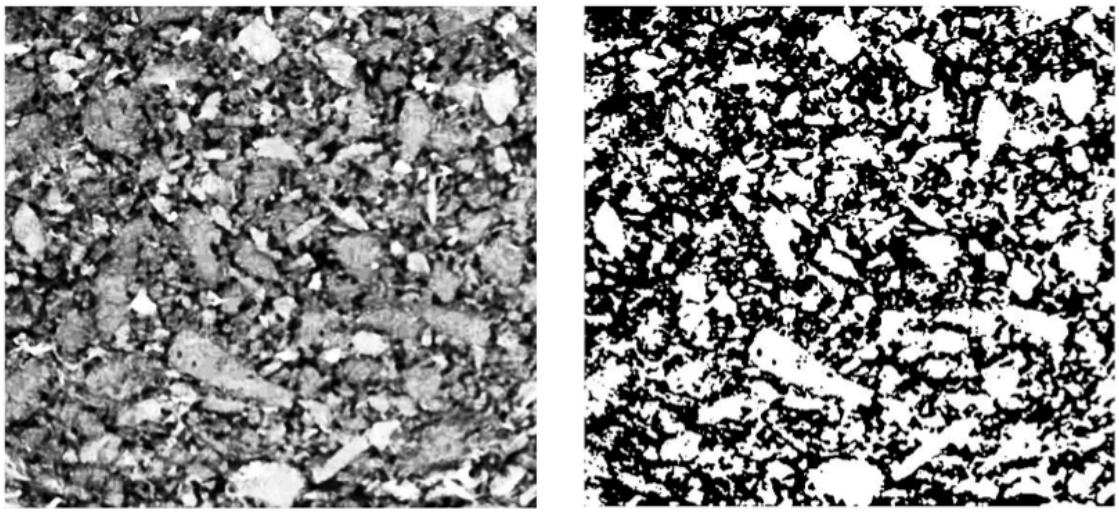

Figure 2.6. Thresholding of a Gray scale Image to Binary Image Using Automated Algorithm.

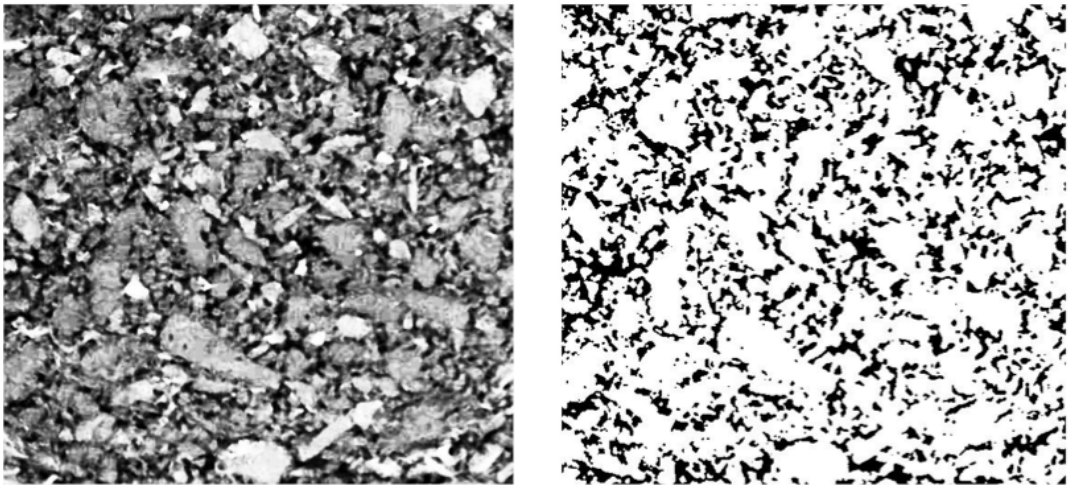

Figure 2.7. Manual Thresholding of a Gray scale Image to a Binary Image.

2.3 IMAGE ANALYSIS

The previous section presented different methods to process raw digital images with the objective of reducing noise and converting a gray scale image to a binary or trinary image that reflect the two or three different components of interest in an asphalt mixture. The next step is to use these images to draw out meaningful information regarding the microstructure of the components within the mix. This section, presents a review of the various metrics and methods that can be used to characterize the internal structure of a composite using three-dimensional X-ray CT images. Section 2.1 introduced some of these metrics that have been used for asphalt mixtures. For example Masad et al., (1999b) quantified aggregate anisotropy using the angle of the major axis of the aggregate to the horizontal axis of the image. The focus of this section will be to review techniques that can be used to quantify the shape characteristics of the matrix (asphalt binder or mastic) in the composite.

Image analysis of a composite generates a variety of measurements on the individual material objects within the composite including volume, orientation, shape, and surface area. A continuous quantity that varies with orientation can be used to quantify the orientation and distribution of material objects within a composite. Examples of such quantities that have typically been used in the literature are mean intercept length (MIL), chord length, star length, and star volume.

One of the simplest direction dependent quantities that can be used to characterize the microstructure of a two-component composite is the mean intercept length (MIL) (Harrigan and Mann, 1984). The MIL along a direction is obtained as follows: grid lines are drawn at specific intervals along the direction on an image of the two-component composite. The intersections between the grid lines and the interface of the two-components are counted. The mean intercept length is then defined as the total length L

of the line grid divided by the number of intersections (Figure 2.8). The MIL can be obtained along several different directions. A drawback of the MIL is that it determines the orientation of the interface rather than the material itself and it may underestimate the anisotropy of the material. An alternative and similar approach is the chord length density distribution. The chord length distribution along a direction is obtained as follows: similar to the MIL grid lines are drawn on an image of the two-component composite and lengths of chords between the intersections of grid lines are measured. The chord length distribution (CLD) function $P(z)$ indicates that the probability of finding a chord of length between z and $z + dz$ is $P(z)dz$ (Torquoato and Lu, 1993).

Two additional direction dependent quantities are the Star Length Distribution (SLD) and Star Volume Distribution (SVD) (Odgaard, 1997a). The star length distribution is calculated by randomly selecting several points in the material of interest within the composite and measuring the length of lines emanating from these points in various directions until the lines encounter a boundary. By doing so, the distribution of the material of interest is obtained. The orientations along which the lines emanate from the points are typically predefined by selecting a homogeneous distribution of points on a unit sphere. Increasing the number of points reduces the uncertainty and is more efficient than increasing the number of orientations. The average star length along a given orientation is computed as:

$$S_w = \frac{1}{n}\sum_{i=1}^{n} L_i \tag{2.1}$$

where, L is the length of measured intercept through point i at orientation w and n is the number of points. The SLD can be obtained for any single material that is of interest

within a multi-component composite (Figure 2.8). The star volume distribution (SVD) is similar to SLD with the only difference that instead of instead a straight line along a particular direction, the volume of a cone emanating from a point in a predefined orientation is measured. The average star volume along any given orientation is computed as:

$$U_w = \frac{\pi}{3n} \sum_{i=1}^{n} L_i^3 \tag{2.2}$$

where, L and n are as described before. The difference between SVD and SLD is that SVD tends to amplify the differences between major and minor components, enhancing the effect of anisotropy. For a more detailed description of these two methods, the readers are referred to (Odgaard, 1997).

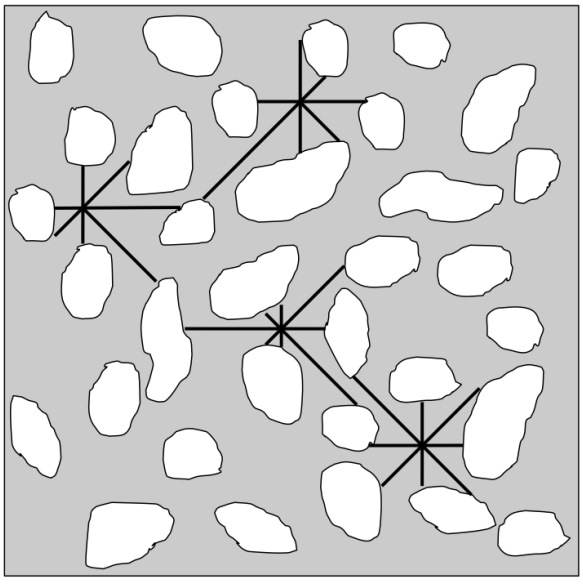

Figure 2.8. Schematic of SLD Measurements at Four Points in a Two-Component Composite.

The aforementioned parameters (MIL, CLD, SLD, and SVD) provide the distribution and mean of a characteristic quantity along different orientations in a composite. A 2D or 3D rose diagram of the mean of any one of these characteristics along different orientations provides an excellent visual representation of the internal microstructure. However, it is also important to use this information to quantitatively derive parameters that relate to the mechanical properties of the composite. One such parameter, that will be used later to characterize the microstructure of sand-asphalt mixtures, is the fabric tensor based on the moment of inertia. Consider that the star lengths are measured at n points along w orientations to produce a data set of N vectors represented by a_i, where $i = 1$ to N.

$$a_i = \begin{bmatrix} a_{xi} \\ a_{yi} \\ a_{zi} \end{bmatrix} \tag{2.3}$$

(Watson, 1966) proposed that the orientation matrix or fabric tensor for this data set is mathematically obtained as follows.

$$T = \sum_{i=1}^{N} a_i a_i^T \begin{bmatrix} \sum_{i=1}^{N} a_{xi}^2 & \sum_{i=1}^{N} a_{xi}a_{yi} & \sum_{i=1}^{N} a_{xi}a_{zi} \\ \sum_{i=1}^{N} a_{xi}a_{yi} & \sum_{i=1}^{N} a_{yi}^2 & \sum_{i=1}^{N} a_{yi}a_{zi} \\ \sum_{i=1}^{N} a_{xi}a_{zi} & \sum_{i=1}^{N} a_{yi}a_{zi} & \sum_{i=1}^{N} a_{zi}^2 \end{bmatrix} \tag{2.4}$$

The orientation matrix or fabric tensor T has three eigen values $\hat{\tau}_1 > \hat{\tau}_2 > \hat{\tau}_3$ and corresponding eigen vectors $\hat{u}_1, \hat{u}_2, \hat{u}_3$ (Watson, 1966);(Ketcham, 2005a). For any axis represented by vector u, the moment of inertia $I(u)$ is given by equation 2.5.

$$I(u) = \sum_{i=1}^{N} |a_i|^2 - u^T T u \tag{2.5}$$

Finally, the eigen vectors $\hat{u}_1$ and $\hat{u}_3$ also represent the direction vectors along which the moment of inertia is minimized and maximized, respectively. The eigen vectors can be used to derive important parameters that reflect the properties of the composite. For example, the degree of anisotropy can be computed as (Ketcham, 2005a):

$$DA = \hat{\tau}_1 / \hat{\tau}_3 \tag{2.6}$$

and elongation index as:

$$EI = 1 - (\hat{\tau}_2 / \hat{\tau}_1) \tag{2.7}$$

These metrics will be used to compare the internal microstructure of the mortar portion of a full-scale asphalt mixture to the internal microstructure of an equivalent FAM specimen.

2.4 Characterization of Mechanical Properties of Mortar Specimens

Mortar specimens comprise asphalt binder and fine aggregates passing #16 sieve. Typically, the test is conducted using a dynamic shear rheometer (DSR) in torsion shear mode. DMA is used in many fields such as engineering, chemistry and polymer physics. This technique is also referred to as forced oscillatory measurements, dynamic mechanical thermal analysis (DMTA), dynamic thermo mechanical analysis or dynamic rheology. DMA can be defined as a technique of applying an oscillatory or pulsing force to a sample. Its importance can be explained by the fact that it provides information on the ability of viscoelastic materials to store and dissipate mechanical energy upon deformation.

In the context of this research, the dynamic mechanical analysis (DMA) of mortar specimens refers to the characterization of damaged and undamaged properties of the mortar. The undamaged properties refer to creep compliance or relaxation modulus of the material as a function of time and temperature or dynamic modulus of the material as a function of frequency and temperature. Damaged properties include rate of plastic deformation, fatigue crack growth, moisture induced damage and also propensity of the material to self-heal. The methods to determine the undamaged properties are well established in the literature. For example, methods to measure and mathematically model the creep compliance or dynamic modulus are well described in the literature (Ferry, 1961; Wineman and Rajagopal, 2000; Lakes, 2009; Brinson and Brinson, 2008). In this study, the dynamic shear modulus and accompanying phase angle were used as indicators of undamaged properties.

There are a number of metrics that have been used to characterize the damage characteristics of mortars or other viscoelastic composites in the literature. A very brief

review of some of these methods is presented below. The discussion is limited to the most common types of distress experienced by bituminous materials.

2.4.1 Plastic deformation in a specimen

Plastic deformation in a viscoelastic material is a function of the load, loading time, and temperature. Typically a series of creep load tests are conducted to measure the recoverable (delayed elastic also referred to as viscoelastic in the context of bituminous materials) and irrecoverable plastic deformation in the material. The resulting response can be mathematically modeled in a form that quantifies the amount of plastic deformation as a function of the load and loading time. There are several mathematical models that are available to achieve this. For example, a mechanical model with a friction element that is characteristic of the yield stress can be used. If the applied stress exceeds the characteristic yield stress of the friction element, the material deforms. Unlike the elastic spring or the viscous dashpot that are also used in the mechanical models, the friction element does not have a well- defined constitutive equation. Therefore, it is typically used in combination with another element. Another approach that is more commonly used is the extension of the classical yield theories or criteria to incorporate time dependency. For an elasto-plastic material a general form of the yield criteria or surface can be written as:

$$f\left(\sigma_{ij}, \varepsilon_{ij}^{p}\right) \geq 0 \tag{2.8}$$

where, σ_{ij} is the stress tensor and ε_{ij}^{p} is the plastic strain tensor used in lieu of the failure stress. For elasto-viscoplastic materials, the time dependency is accommodated by using an additional parameter. For example equation 2.8 can be modified as follows:

$$f\left(\sigma_{ij},\varepsilon_{ij}^{p},\tau_{ij}\right) \tag{2.9}$$

where, the term τ_{ij} adjusts the yield criterion accordingly to accommodate for the viscoelastic nature of response. One example is the Nagdi-Murch model that defines this term as follows:

$$\tau_{ij} = \tau_{ij}(\varepsilon_{ij}^{v} - \varepsilon_{ij}^{e}) \tag{2.10}$$

where, $\varepsilon_{ij}^{v}$and ε_{ij}^{e} denote the time dependent and elastic strains, respectively. (Crochet, 1966) defined the time dependent function to be a scalar of the form:

$$\tau = \sqrt{(\varepsilon_{ij}^{v} - \varepsilon_{ij}^{e})(\varepsilon_{ij}^{v} - \varepsilon_{ij}^{e})} \tag{2.11}$$

More recently, Masad and co-workers have used the Schapery's nonlinear viscoelastic model to characterize the nonlinear viscoelastic and viscoplastic strain in asphalt materials (Masad et al., 2008; Huang et al., 2007). They were able to quantify the evolution of plastic strain in the asphalt specimen by accounting for stress history and the delayed elastic or viscoelastic strain from a multiple creep load test.

2.4.2 Fatigue crack growth

Cyclic or monotonic load tests are typically conducted to determine fatigue cracking or fracture resistance of the material. Most of the work related to crack growth in bituminous materials is centered on two approaches; the energy-based path-

independent integrals and the cohesive zone model. Cherepanov, (1968) and Rice, (1968) developed the energy based integral approach, now commonly referred to as the J-integral approach, to define the work done per unit area of crack growth. Schapery (1975a; 1975b; 1975c; 1984) used the energy-based path independent J-integral for non-linear elastic and plastic materials in conjunction with correspondence principles to derive an expression for crack initiation and crack growth in a viscoelastic media.

Masad et al., (2006) used the correspondence principle proposed by Schapery, (1984) and the DMA to characterize fatigue damage in mortars. DMA samples were compacted and cored according to the procedure described by Zollinger, (2005). DMA tests were performed under controlled-strain and controlled-stress modes of loading, 25°C, and 10Hz frequency. The tests were done in two stages: a low amplitude test was conducted to determine the undamaged or linear viscoelastic properties followed by a high amplitude test to induce fatigue cracking. The authors observed that controlled-strain and controlled-stress tests develop fatigue cracking in a different way. Under controlled-strain, the strain is kept constant and the stress decreases during the test. The dynamic modulus decreases, while the phase angle increases. These two modes of testing have an opposite influence on the area of the hysteresis loop (the fact that the dynamic modulus decreases makes the area of the hysteresis loop to decrease and the fact that the phase angle increase makes the area of the hysteresis loop to increase). The net effect is that in controlled-strain the hysteresis loop area decreases during the test and under controlled-stress test conditions, both manifestations of damage (decrease in stiffness and increase in phase angle) have the same effect; increase the hysteresis loop area. The approach proposed by these authors was to separate the dissipated energy due to the fatigue damage into three main sources: (i) the change in the phase angle (WR1), (ii) permanent deformation involved in the process (WR2) and (iii) the change in the mix

stiffness (WR3). The authors found that using intermediate values of dynamic modulus and phase angle (within the nonlinear region) as the viscoelastic properties (VE) they were able to separate the effects of the nonlinear material behavior and the damage. Bhasin et al., (2009) compared the use of various energy-based methods to quantify the rate of fatigue crack growth in asphalt mixtures.

2.4.3 Moisture damage

The presence of moisture in mortar or asphalt mixture specimens amplifies other forms of distress such as fatigue crack growth. The moisture damage potential of mortar specimens is typically determined in conjunction with the fatigue crack growth. Zollinger, (2005) compared the fatigue cracking resistance of moisture-conditioned specimens to unconditioned specimens using the DMA in order to evaluate their moisture damage resistance. Moisture conditioning was achieved by allowing moisture to penetrate the specimen by placing it in distilled water and applying vacuum to accelerate moisture penetration. The specimen was retained under water and vacuum for one hour. Zollinger, (2005) reported that the saturation computed as the volume of water absorbed to the volume of air voids, was approximately 125 percent indicating that some of the moisture diffused into the binder or aggregate matrix. Caro et al., (2008) used a similar approach to characterize the moisture damage resistance of mortar specimens. They compared the performance of moisture-conditioned specimens to unconditioned specimens and quantified the moisture damage resistance using a probabilistic approach.

2.4.4 Healing potential

Some of the recent work on the laboratory investigation of healing can be attributed to (Little et al., 2001; Kim and Roque, 2006; Carpenter and Shen, 2006; Maillard et al., 2004). These studies clearly demonstrate the evidence for existence of healing and its significant impact on the fatigue cracking life of asphalt mixtures. Little et al., (2001) applied a rest period of 24-hours in traditional flexural beam bending experiments resulting in the increase of fatigue life by more than 100 percent depending on the type of binder used. Kim and Little (2005) used torsion loading on asphalt mastics to demonstrate similar results. They observed that the impact of healing is by far the greatest when rest periods are applied before significant damage occurs. Carpenter and Shen, (2006) used dissipated energy between load cycles to quantify healing. They verified this observation by demonstrating that the application of short rest periods between each load cycle not only extends fatigue life, but also is responsible for the extension of so called "endurance limit" of some asphalt mixtures. Kim and Roque, (2006) quantified healing in terms of the recovered dissipated creep strain energy per unit time by using a similar approach to that of Carpenter and Shen, (2006). Maillard et al., (2004) simulated the conditions in which an asphalt film is bound by aggregates by conducting tensile tests on films of asphalt binders lodged between glass spheres. Rate of healing in the asphalt was measured by transmitting ultrasonic waves through the sample. A decrease in the amplitude of the ultrasonic signal corresponds to damage in the film whereas an increase in the amplitude corresponds to the healing process.

Similar to the work of Kim and Little, (2005), Bhasin et al., (2008) quantified the healing potential of different FAM mixtures using the DMA. They applied cyclic loads to FAM specimens using a DMA and introduced nine rest periods of four minutes each during the cyclic test. The rest periods were introduced after cycles that correspond to

2.5, 5, 10, 15, 20, 25, 30, 40, and 50 percent of the fatigue life value for that particular material, as measured without any rest period. When rest periods were applied, the parameter, b, was computed as the slope of the dissipated energy versus ln number of load cycles. The parameter b determined without the rest period was then compared to the parameter b determined with rest periods. A relative decrease in this parameter, which would be associated with positive healing, was then used to quantify the healing potential for each material.

In this study, the DMA is used to evaluate whether the method of compaction used to fabricate FAM specimens has any influence on its mechanical properties and to evaluate the influence of mixture design characteristics such as gradation and binder content on the performance of the FAM specimens. Due to the limited scope, not all the metrics described in the aforementioned sections were included in this study. A summary of parameters that were used to compare the microstructure and engineering properties of the specimens is listed below. A more detailed description on how these metrics were obtained for the selected materials is presented in Chapter 4.

Parameters for the full-scale asphalt mixture specimens as well as the FAM specimens based on the image analysis of microstructure include the following.

1. Degree of anisotropy (equation 2.6).
2. Average star length along the principal direction (equation 2.1).
3. Average coefficient of variation of the star lengths along all directions.
4. Orientation of the principal direction (equation 2.4).

Parameters for the FAM specimens based on the mechanical tests include:

1. Undamaged shear dynamic modulus or G* and phase angle.

2. Rate of crack growth from a fatigue test.
3. Healing characteristics during long rest periods.

Chapter 3. Materials, data collection and processing

3.1 Selection of Materials and Specimen Fabrication

The first objective of this study was to identify metrics that can be used to quantify the shape characteristics and variability in the microstructure of asphalt or mastic matrix in an asphalt mixture. A secondary objective of this study was to evaluate the influence of mixture properties and methods of compaction on the properties of the FAM and also to compare the microstructure of the FAM specimen to the microstructure of the FAM portion of a corresponding full-scale asphalt mixture. To achieve these two objectives of this study, a typical dense-graded asphalt mixture was selected. Three additional variations of this mixture were produced in the laboratory by changing the binder content, coarse aggregate gradation, and fine aggregate gradation to produce a total of four different mixtures. The four mix designs were labeled as control, high binder, coarse adjusted, and fine adjusted. The aggregate used in all mixtures was a limestone obtained from RTI South Plant, Buda, Texas. Limestone is well suited for X-ray CT scanning because of its relatively homogeneous mineral makeup compared to other aggregates. Although igneous aggregates or gravels may also be used, these aggregates typically contain minerals with varying densities that may result in non-uniform X-ray attenuation and artifacts in the CT images. The asphalt binder had a performance grade of PG 64-22.

Figure 3.1 illustrates the gradation and binder content for these four mixtures. The gradation limits were based on the specification followed by the Texas Department of Transportation (TxDOT) for Type C mixtures and all variations of the control mix were

designed to be within these limits. The control mix had 4.2% binder content by weight of aggregates, and the high binder mix had 4.7% binder content but the same aggregate gradation as the control mix. The coarse adjusted mix had the same binder content and fine aggregate (passing #16 sieve) gradation as the control mix but the gradation of the coarser aggregates (retained on #16 sieve) was modified. Similarly, the fine adjusted mix had the same binder content and coarse aggregate gradation as the control mix but the fine aggregate gradation was modified. Three different types of FAM mix designs were also developed corresponding to the control (labeled as Mix 1), high binder (labeled as Mix 2), and fine adjusted (labeled as Mix 3) full-scale mixtures. A FAM mix design for the coarse adjusted full-scale mixture was not developed for the following reason. The coarse adjusted mix had a gradation that was adjusted only in the coarse aggregate fraction (aggregate retaining on #16 sieve) as compared to the control mix. In other words, the gradation of the aggregates passing #16 sieve was the same for the coarse adjusted mix as well as the control mix. As a result, the gradation for the FAM mix corresponding to both these mixtures is the same. Appendix A presents an example illustrating the methodology that was used to determine a FAM mix design corresponding to the design of a full-scale asphalt mixture. Figure 3.2 illustrates the gradations for the three FAM mixtures.

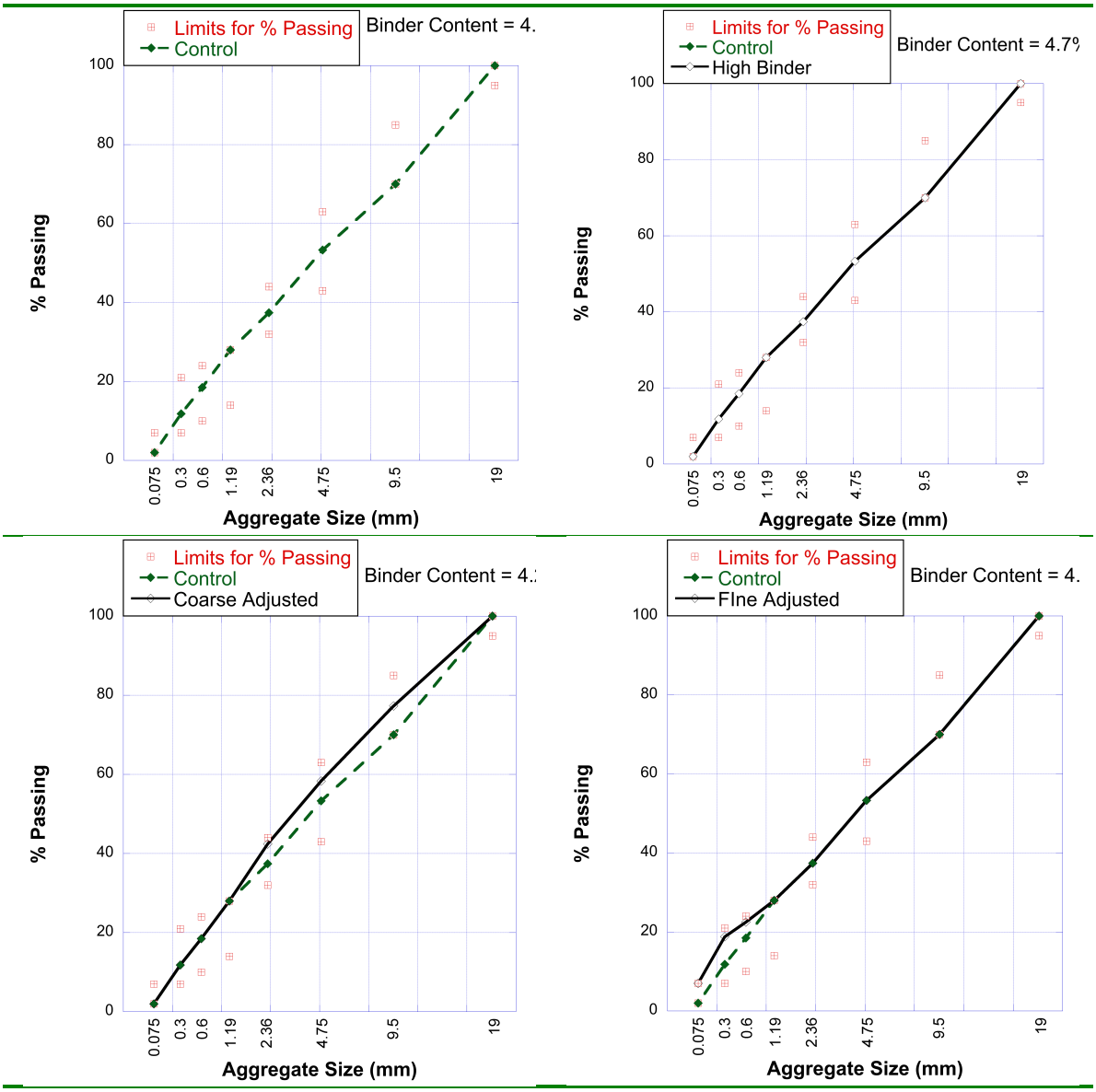

Figure 3.1. Gradations for the Four Different Full-scale Asphalt Mixtures.

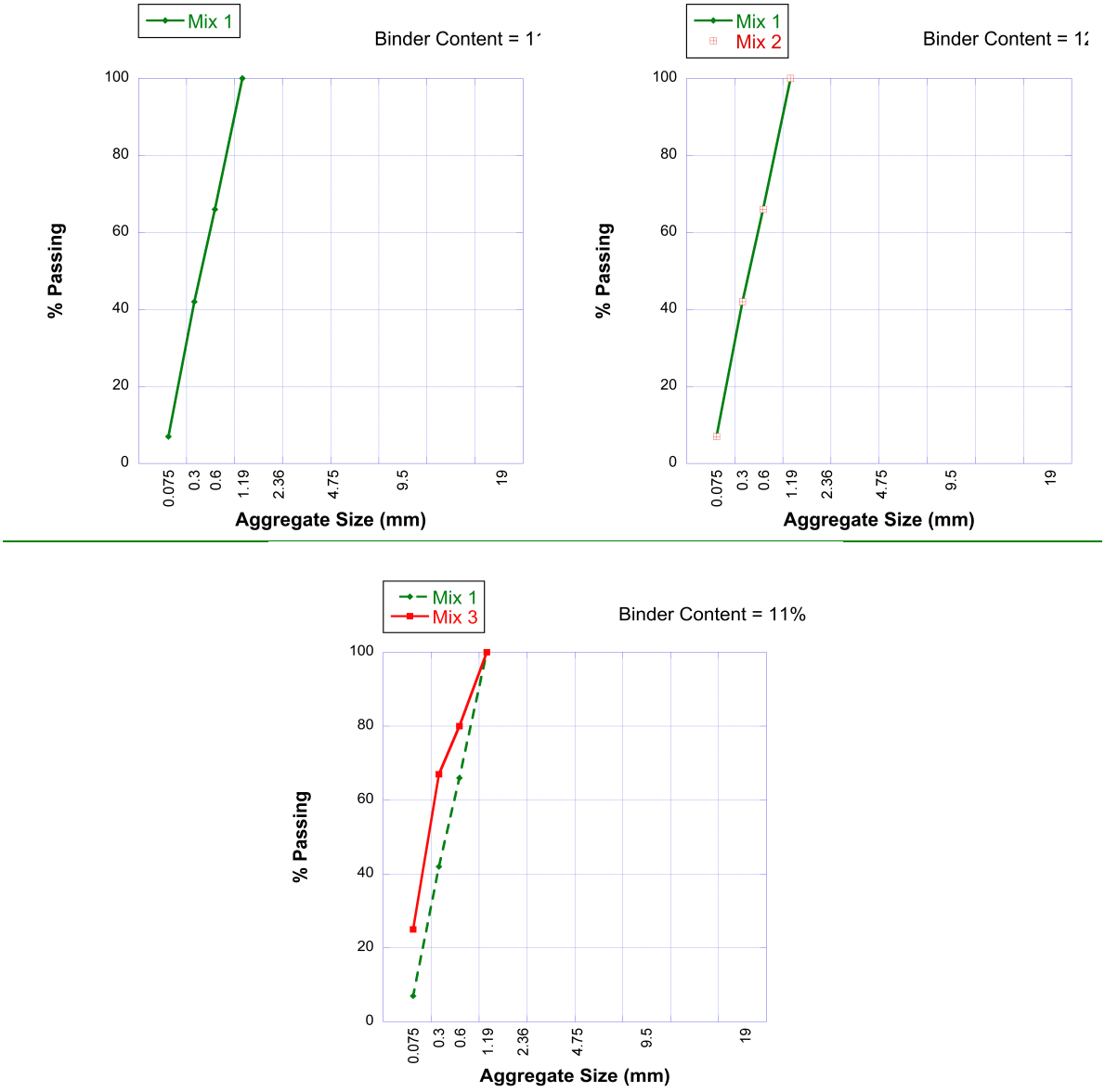

Figure 3.2. Gradations for the Three Different FAM Mixtures.

It is important to emphasize that all four mixes used the same binder and aggregate and the only difference between the control and other mixes was either the binder content or the gradation. The rationale for selecting these four mixtures was to evaluate the influence of binder content and gradation on the properties of the FAM specimen as well as to compare the microstructure of the FAM specimen to the microstructure of the FAM within a corresponding full-scale asphalt mixture.

The maximum specimen size that can be used with the three dimensional X-ray CT scanner is dictated by the resolution required for microstructure characterization. A resolution in the range of 15 micrometers per voxel was considered as appropriate for this study. A cylindrical specimen approximately 12.5 mm in diameter was considered as appropriate to achieve this resolution. This specimen diameter was also appropriate for the mechanical testing using the DMA. The following procedure was used to obtain specimens for the full-scale asphalt mixture for X-ray CT scanning and specimens for FAM mixtures for X-ray CT scanning and DMA testing.

Full-scale asphalt mixture specimens for each of the four mixture types were compacted using the Superpave gyratory compactor (SGC). The specimens were 152 mm in diameter and 100 mm in height. The ends of the SGC compacted specimen were cut using a diamond blade saw to achieve a finished specimen height of 50 mm. A diamond-coring bit was used to core approximately ten specimens that were half inch in diameter and 50 mm in height. Two specimens cored from the SGC compacted specimen for each type of mixture were selected for X-ray CT scanning. The two cored specimen were selected such that they had similar air void content as compared to the average air void content of the SGC compacted specimen.

The cylindrical FAM test specimen comprised of the bitumen mixed with fine aggregate (material passing #16 sieve). The aggregates and the bitumen were mixed at the specified mixing and compaction temperature using a mechanical mixer. After short term aging for two hours, the mix was compacted using three different methods.

The first method was to use a 152 mm diameter mold with the Superpave gyratory compactor to compact a specimen with a height of 75 mm and target air void content of 13%. The compacted samples were allowed to cool to room temperature. Each side of the compacted sample (top and bottom) was trimmed to obtain a sample height of 50 mm. Approximately 30 FAM test specimens of 12.5 mm diameter were obtained by coring the 152 mm diameter compacted sample. FAM specimens from the inner core of the SGC compacted specimen were separated from the specimens from the outer core of the SGC compacted specimen. Figure 3.3 illustrates the schematic of these specimens.

The second method was to use a beam compactor. The short-term aged loose mix was compacted using a beam compactor and test specimen. The beam specimen was trimmed by about 15 mm from all sides to reduce end effects. FAM test specimens were then cored from the beam specimen by coring in the direction of compaction as well as perpendicular to the direction of compaction. Figure 3.4 illustrates a schematic for the FAM specimens obtained using the beam compacted specimen.

The third and last method of compaction was to use a Marshall compactor. The procedure was the same as the SGC specimen but the FAM specimens obtained only from the middle part of the specimen and hence there were no inner or outer core specimens. It must be noted that all specimens were compacted until refusal, i.e. the compaction effort was applied until such time that no change in the volume of the specimen was observed.

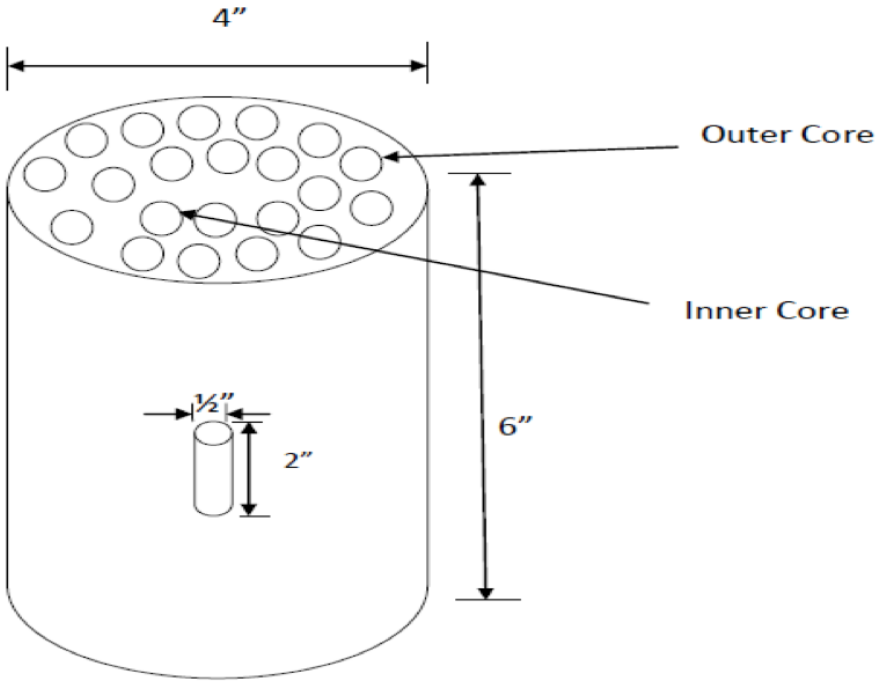

Figure 3.3. Schematic of FAM Specimens Cored out of SGC Specimen.

3.2 HIGH RESOLUTION X-RAY CT SCANNING OF IMAGES

The finished full-scale mix and FAM specimens were used to obtain high-resolution sectional images for a volume of interest. The scanning was performed at the high-resolution X-ray CT Facility at the University of Texas at Austin (UTCT). Ketcham and Carlson, (2001) provide a more detailed description of the principles of X-ray tomography and methods used to acquire images and correct artifacts. In summary, high-resolution X-ray CT scanning (HRXCT) is based on the principle that an X-ray fan beam

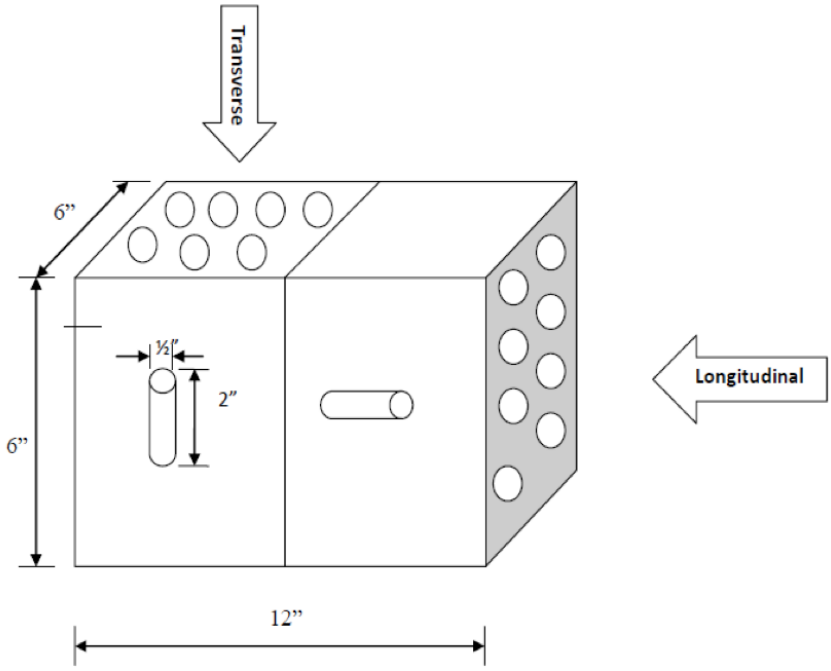

Figure 3.4. Schematic of FAM Specimens Cored out of Beam Specimen.

(or cone beam) is directed at an object from all orientations in a plane, and the decrease in X-ray intensity caused by passage through the object is measured by a linear array of detectors (Figure 3.5). The resulting data are then reconstructed to create a cross-sectional image of the object along that plane. The gray scales in such images reflect the relative linear X-ray attenuation coefficient μ, which is a function of density, atomic number, and X-ray energy. For this study, the energy source used was adjusted to 80kV and 10W to obtain the best resolutions.

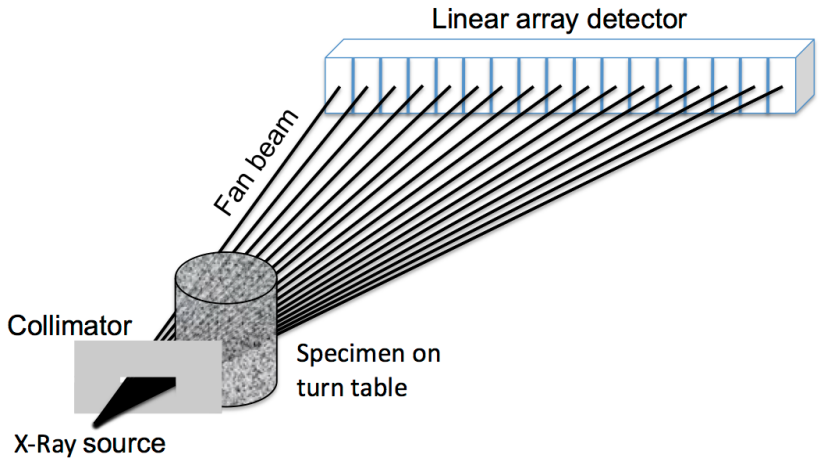

Figure 3.5. Schematic of X-Ray CT Imaging. (Adapted from Ketcham, 2005a)

Each CT image is termed a 'slice', as it corresponds to what one would see if the object were sliced along the scan plane. By gathering a stack of contiguous slices, data for a complete 3D volume can be obtained. Each slice represents a finite thickness of material, corresponding to the thickness of the collimated X-ray beam and detector array. Consequently, the pixels in CT images represent volume elements and are referred to as voxels (Ketcham, 2005b).

For the full-scale asphalt mixture, two specimens for each of the four types of mixtures were scanned using the HRXCT for a total of eight full-scale mix specimens. For the FAM mixtures, 10 specimens for each of three types of mixture were scanned using the HRXCT for a total of 30 FAM specimens. For each mixture design the 10 specimens comprised two from the inner core of the SGC compacted specimen, two from the outer core of the SGC compacted specimen, two from the beam specimen cored along the direction of compaction, two from the beam specimen cored along the transverse direction, and two from the Marshall compacted specimen. For each of the full-scale or

FAM specimens, a volume approximately 15 mm x 15 mm x 8 mm, enclosing the middle third of the specimen was scanned to obtain a total of 562 images each with a resolution of 1024 x 1024 pixels. The problems of beam hardening and ring artifacts were removed during post-construction phase. Figure 3.6 shows the typical matrix with scans of the specimen.

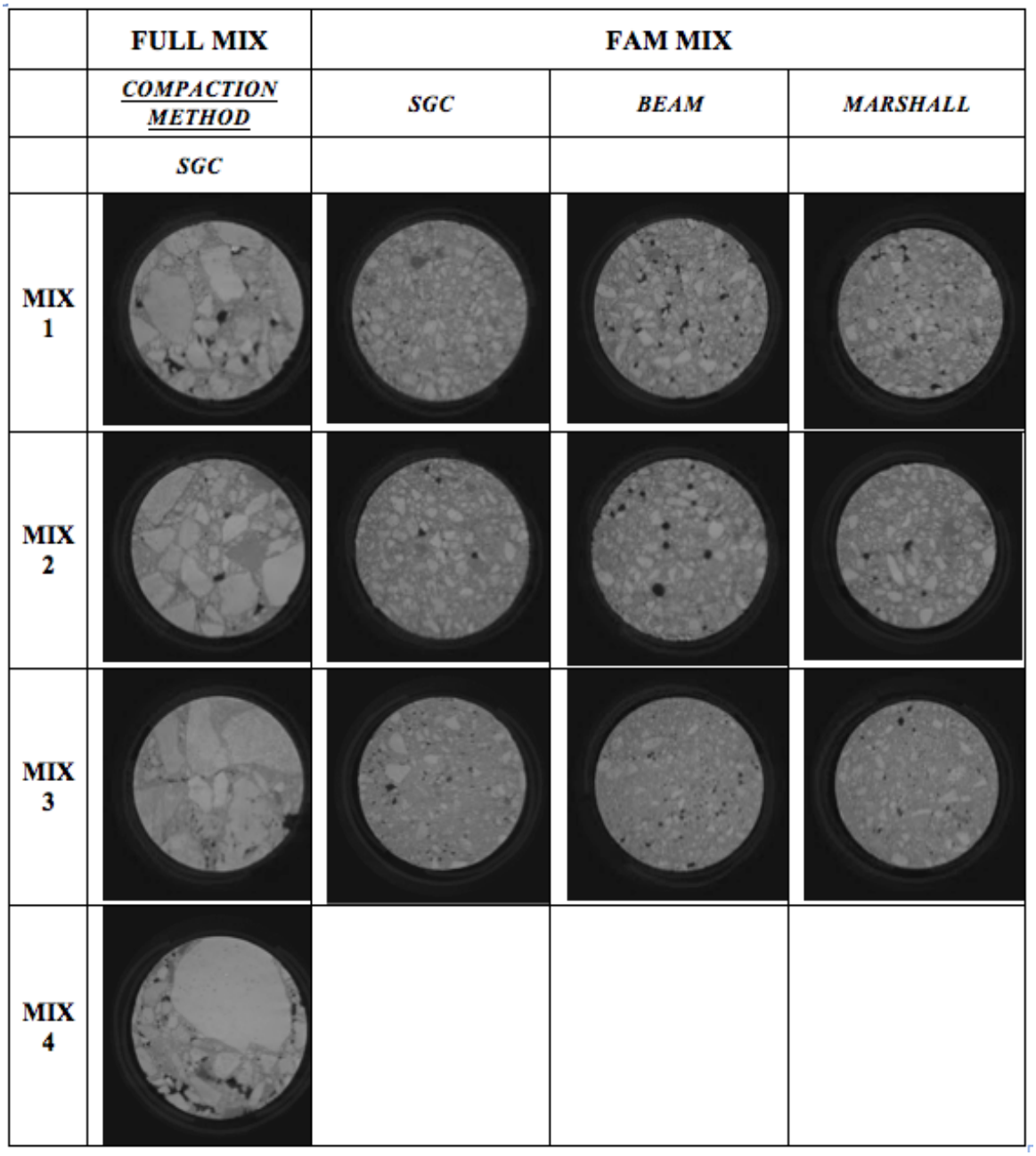

Figure 3.6. Typical Slice Scans and Test Matrix.

3.3 IMAGE PROCESSING

All images acquired using the HRXCT must be processed before conducting any kind of analysis. Matlab was used to process the images by cropping the images, removing noise and running a thresholding algorithm to separate the three components in the composite, i.e. mastic, air void and aggregate. The steps used for the image analysis are briefly described here. The two dimensional slice images obtained after scanning were 1024x1024 pixels in size. The images were cropped to a size of 512x512 pixels to obtain the region of interest and remove any unwanted information from the edges. The pixel intensity values of the images obtained in this manner varied from 0 to 165. In order to examine the fine details and visually distinguish between the fine features it is important to fully utilize the entire range of intensity values, i.e. 0 to 255. Therefore a contrast enhancement operation was performed on the cropped images.

All digital images, including the ones used in this study, contain some amount of noise. Eliminating noise while preserving the details of interest in the image is one of the challenges in image processing. Several different types of linear and nonlinear filtering tools are available to remove different types of noise that is typically present in digital images. Regardless of the type of filter, the output image should minimize noise without destroying the information of interest in the image. The first step to eliminate noise is to identify the type of noise in the image. Multiplicative noise is usually associated with a blur that was not seen in the images. The digital noise in the images was most likely an additive noise. Using linear and nonlinear filters can reduce this kind of noise. However, linear filters are not the best choice for this study because it is associated with blurring of images and loss of detail at the edges. Figure 2.3 illustrates this for the neighborhood average filter, which is a linear noise filter. Therefore, several different types of non-linear filters were applied to the images (e.g. median filter and anisotropic diffusion).

Several images were used with these filters and visually compared. Based on this comparison it was found that the median filter was most effective in reducing noise and preserving details. As described before, in median filtering the gray level of each pixel is replaced by the median of the gray level of all pixel values in the pixel's neighborhood (Russ, 2007). The neighborhood area, which is also referred as the kernel, used in this study, was 3 by 3. Figure 2.4 demonstrates the use of median filter on a sample image.

A typical mixture composite can be broken down into three components – aggregates, mastic (binder with fines or aggregates finer than 75 microns), and air. After noise reduction the next step was to convert the grayscale image to an image that contained only three pixel intensity values representing the three components within the composite. A thresholding operation was performed such that the end product had air represented by black pixels (pixel value 0), mastic represented by gray (pixel value 150) and aggregate represented by white (pixel value 255). The objective of the thresholding operation is to identify two pixel intensity values in the gray scale image that differentiate between these three components. The volumetric properties (volume of air void and volume of mastic) of each specimen were determined. An iterative process was used to determine the two pixel intensity values that differentiated between air voids, mastic, and the aggregates for a stack of 520 images that represent a volume of the specimen. The iterations were designed to minimize the difference between the volume percent of air voids and mastic computed using the stack of images to the values obtained experimentally. This procedure was based on the work of Zelelew et al., (2008). The thresholds were defined when the computed volume of the mastic and air voids were within a certain tolerance of the known volumes for the mixtures. Since characterizing the microstructure of the mastic between coarse aggregate particles was one of the objectives of this study, a greater emphasis was placed on achieving the correct volume

percentage of the mastic. Also, the volume of the specimen that was imaged was a small portion of the specimen that was used to obtain volumetric air content. Therefore, it is possible that the computed values for the air void content from the stack of images may not closely match the air void content of the entire specimen. For this reason, a broader tolerance was used to compute the threshold for the air void content.

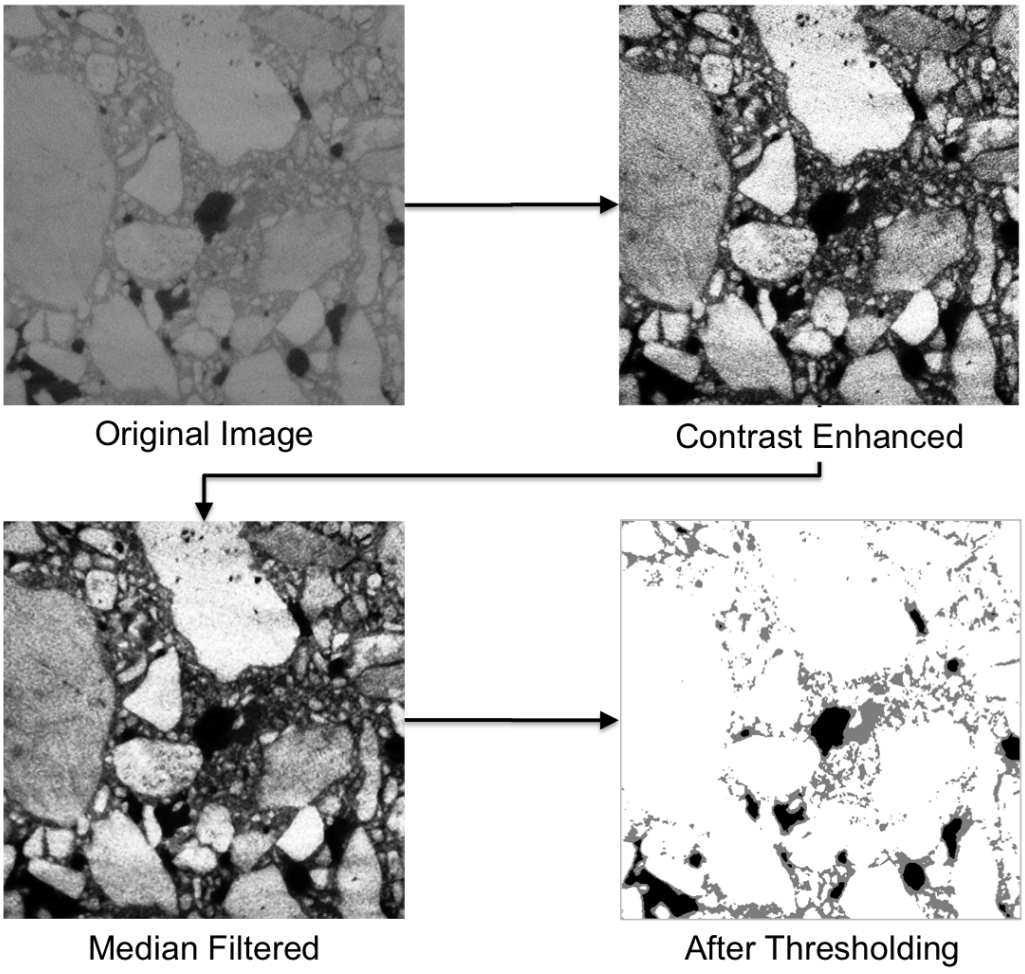

Figure 3.7. Schematic of Image Processing Steps.

Chapter 4. Analysis and results

4.1 Analysis to Determine the Microstructure of the Asphalt Matrix

One of the objectives of this study is to establish quantitative metrics to characterize the three dimensional microstructure of the asphalt binder or matrix in an asphalt mixture and then to compare the microstructure of the mortar within a full-scale asphalt mixture specimen to the microstructure of a corresponding FAM specimen. Based on a literature review, the metric of choice selected for this study was the fabric tensor obtained using the star length distribution (SLD). The Quant3D program originally developed by Ketcham and co-workers was used for analyzing images and characterizing the microstructure of the mastic (Ketcham, 2005b). The Quant3D program uses the processed images as an input and computes the SLD (or SVD), fabric tensor, eigen values and eigen vectors for the component of interest. The SLD provides the average length of the component of interest (for specified number of points) along different orientations using a three-dimensional rose diagram. For this study, it was also of interest to examine not only the average length but also the distribution of this length along each orientation. Therefore the program was slightly modified to report the distribution of the lengths along each orientation.

Figure 4.1 illustrates the user interface for the Quant3D program. For each specimen 512 processed slice images were uploaded. The critical inputs for this program are as follows. The threshold range of values is used to describe the component of interest. For example, in the processed images, the air voids, mastic, and aggregates are represented using pixel intensity values of 0, 150, and 255, respectively. For example, in

order to analyze the microstructure of the mastic, a range of 145-155 can be used. The number of directions is used to define the number of orientations along which the lengths will be measured. For this study, 513 orientations that represent a uniform distribution on a sphere were selected. A total of 1000 points were randomly selected to make these measurements. Choosing the appropriate number of points is an important parameter to obtain meaningful results. Selection of too many points results in very long computing time. In contrast, selection of too few points will not provide meaningful distributions.

Figures 4.2 and 4.3 illustrate the typical three-dimensional rose diagram for the SLD and SVD, respectively. The average SLD is used to compute the fabric tensor using equation 2.4. The eigen vector and eigen values for this fabric tensor are also computed. Recall that the eigen vectors with the largest and smallest eigen values represent the direction vectors along which the moment of inertia is minimized and maximized representing the preferred direction of the matrix. In addition, the ratio of the maximum to the minimum eigen values is a measure of the degree of anisotropy. Table 4.1 lists the fabric tensor, eigen values, and eigen vectors based on a typical SLD analysis.

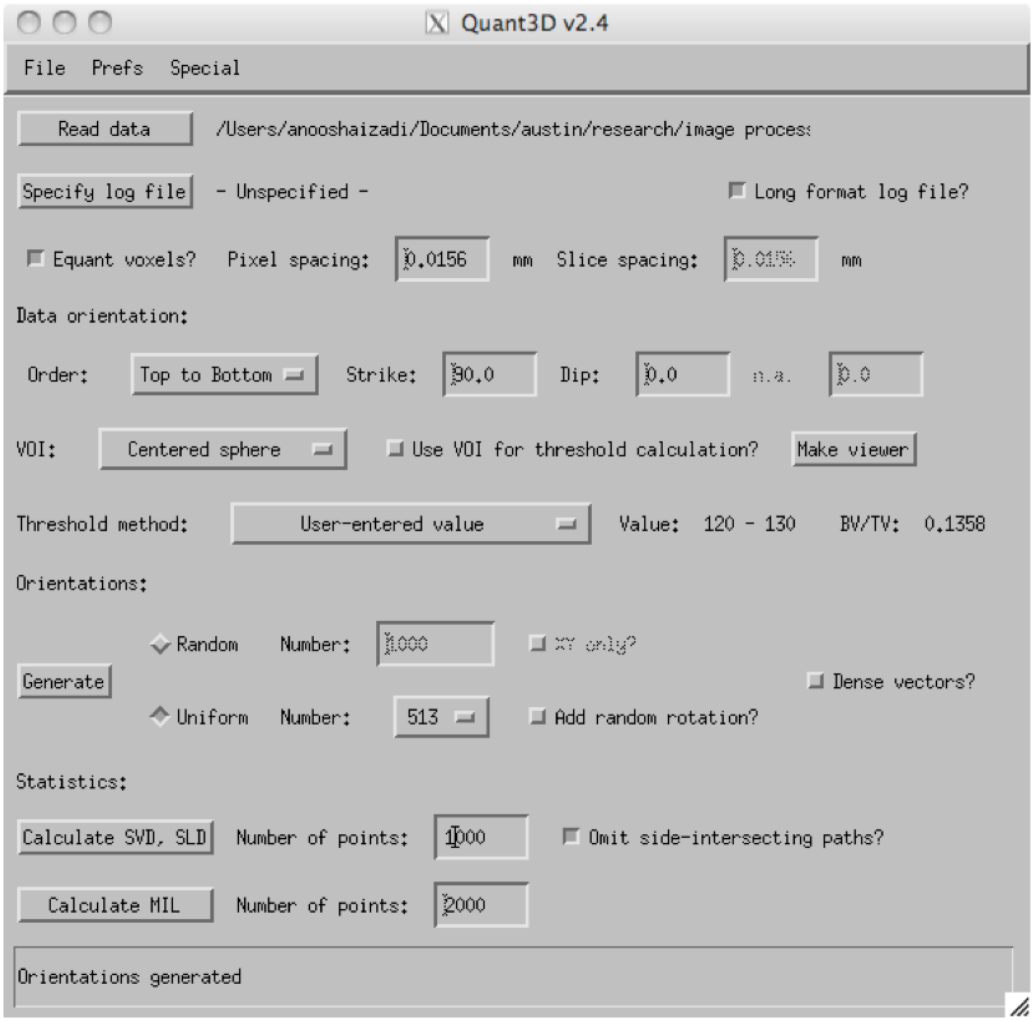

Figure 4.1. Interface for the Quant3D Program.

In summary, the analysis based on SLD provides the following information:

- average three dimensional geometry of the asphalt matrix,
- orientation of this geometry with respect to the direction of compaction of the mixture, and
- the degree of anisotropy in the matrix between particles.

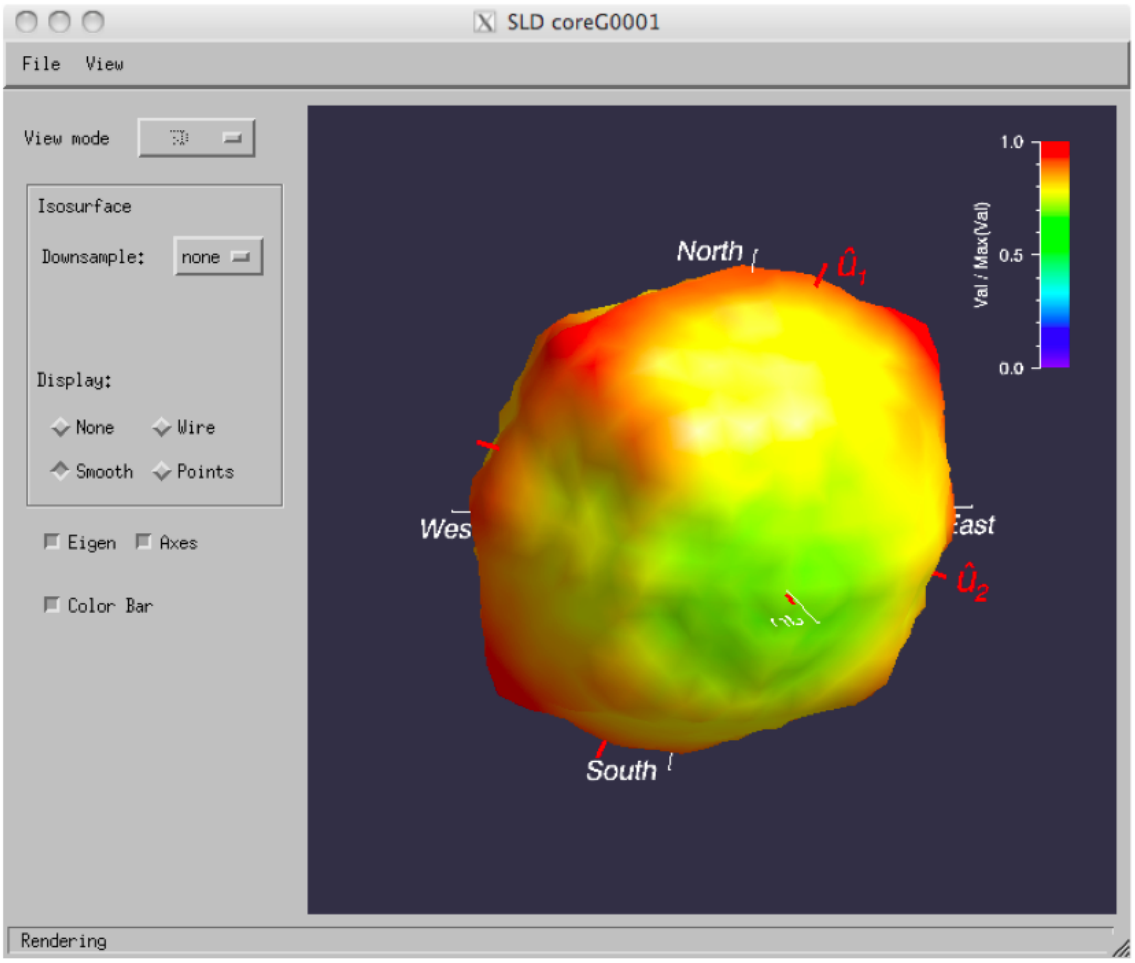

Figure 4.2. Typical Three Dimensional Rose Diagram for SLD from Quant3D.

Although the above analysis provides the average three-dimensional geometry of the matrix between aggregate particles, it does not provide information about the variability in the geometry. The following section describes the methods used to characterize the variability in the microstructure of the asphalt matrix.

4.2 VARIABILITY IN THE MICROSTRUCTURE OF THE MATRIX

The Quant3D program was modified to provide star lengths at each one of the 1000 points along the 512 directions used in this study. The next was to determine the

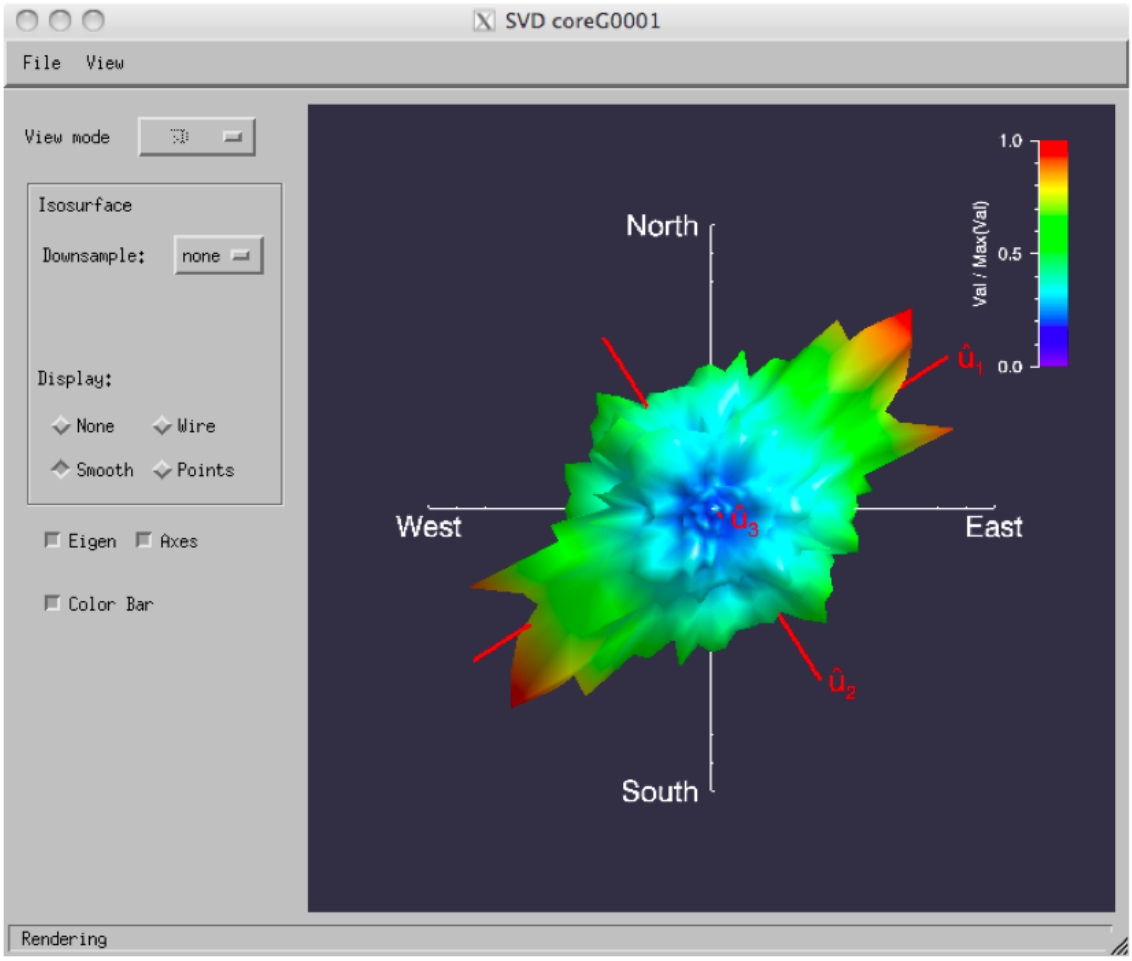

Figure 4.3. Typical Three Dimensional Rose Diagram for SVD from Quant3D.

distribution of the star length along a given direction. A frequency histogram of the star lengths along each direction was plotted. It was found that the Weibull distribution was a reasonably good representation of the distribution of star lengths along each one of the directions. The Weibull distribution has two parameters, shape and scale, that can be

varied to fit a wide variety of observed data. The Matlab program was used to obtain the parameters for the Weibull distribution using the 1000 points along each one of the 512 directions. Figure 4.4 illustrates the typical distribution of the star length and the Weibull distribution that was fit using Matlab. The shape and scale parameters for the Weibull distribution were then used to compute the standard deviation and coefficient of variation of the star length along each direction.

The coefficient of variation along different directions were used to plot a three dimensional rose diagram to assess whether or not any particular direction was more susceptible to variability than others (Figure 4.5). This is similar to the rose diagram for the star length distribution, with the difference that the coefficient of variation was used to plot the three-dimensional rose diagram. In addition, an average coefficient of variation was also computed for all the 512 directions to be used as a metric to compare the variability of the microstructure between different mixture types.

Table 4.1. Typical Results From Quant3D for SLD Analysis.

Parameter	Value
Fabric Tensor Based on SLD	$\begin{bmatrix} 0.351 & 0.006 & -0.0008 \\ 0.006 & 0.344 & -0.0006 \\ -0.0008 & -0.0006 & 0.3042 \end{bmatrix}$
Eigen vectors	$\begin{bmatrix} 0.8635 & 0.5040 & -0.0191 \end{bmatrix}$
	$\begin{bmatrix} 0.5042 & -0.8636 & 0.0036 \end{bmatrix}$
	$\begin{bmatrix} -0.0147 & -0.0128 & -0.9998 \end{bmatrix}$
Eigen values	0.3551
	0.3407
	0.3042
Degree of Anisotropy	1.1672

4.3 IMAGE ANALYSIS RESULTS

The results were used to obtain the four parameters that describe the internal microstructure or dimensional distribution of the mastic with the full-scale asphalt mixture as well as the FAM specimens. These four parameters are described below:

- Degree of anisotropy: This is defined as the ratio of the maximum to the minimum eigen values.
- Average star length along the preferred direction: The preferred direction is the principal direction that has the highest eigen value. It is also the direction along which the moment of inertia of the geometry is minimized.

- Average variation in the star lengths along all directions: The analysis was conducted by measuring the star lengths along 513 orientations at 1000 points. The average of the 1000 star lengths along each direction is used to obtain the average three-dimensional shape of the matrix. Similarly, the standard deviation along each of these 513 directions can be computed for the 1000 points. Since the standard deviations along different directions did not vary significantly, the average of the standard deviations and average of the coefficient of variation along the 513 directions were computed and compared for different mixes.

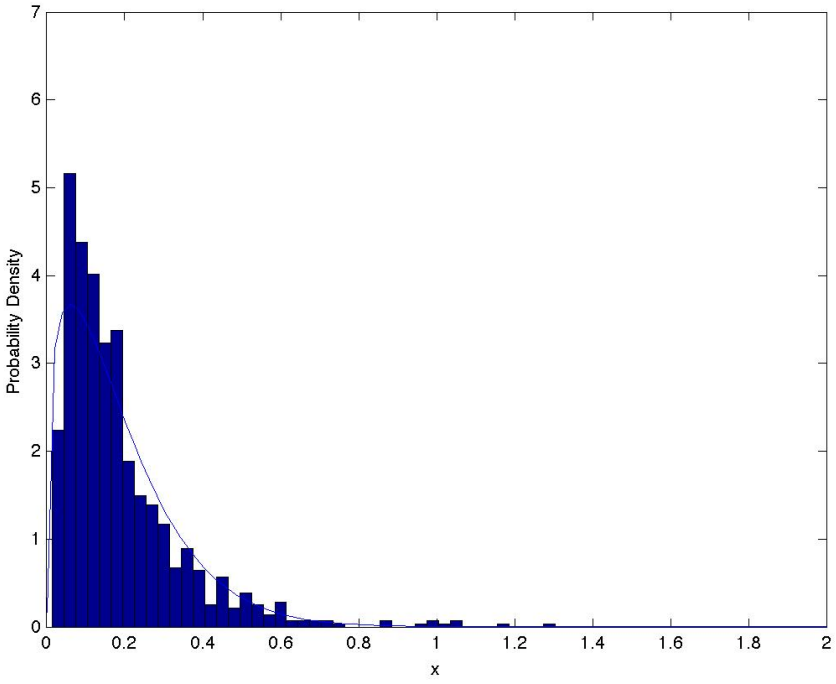

Figure 4.4. Typical Distribution of the Star Length Along a Given Direction.

- Orientation or preferred direction of the mastic: This refers to the orientation of the eigen vector with the highest eigen value or lowest moment of inertia. This is also the orientation along which the maximum value of the star length is aligned. The orientation or plunge is the angle made by the vector that defines the preferred direction to the plane perpendicular to the direction of compaction (Figures 4.6 and 4.7).

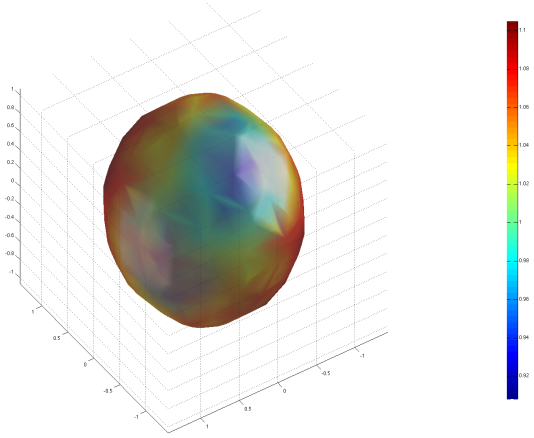

Figure 4.5. Three Dimensional Rose Diagram for the Coefficient of Variation of Star Lengths.

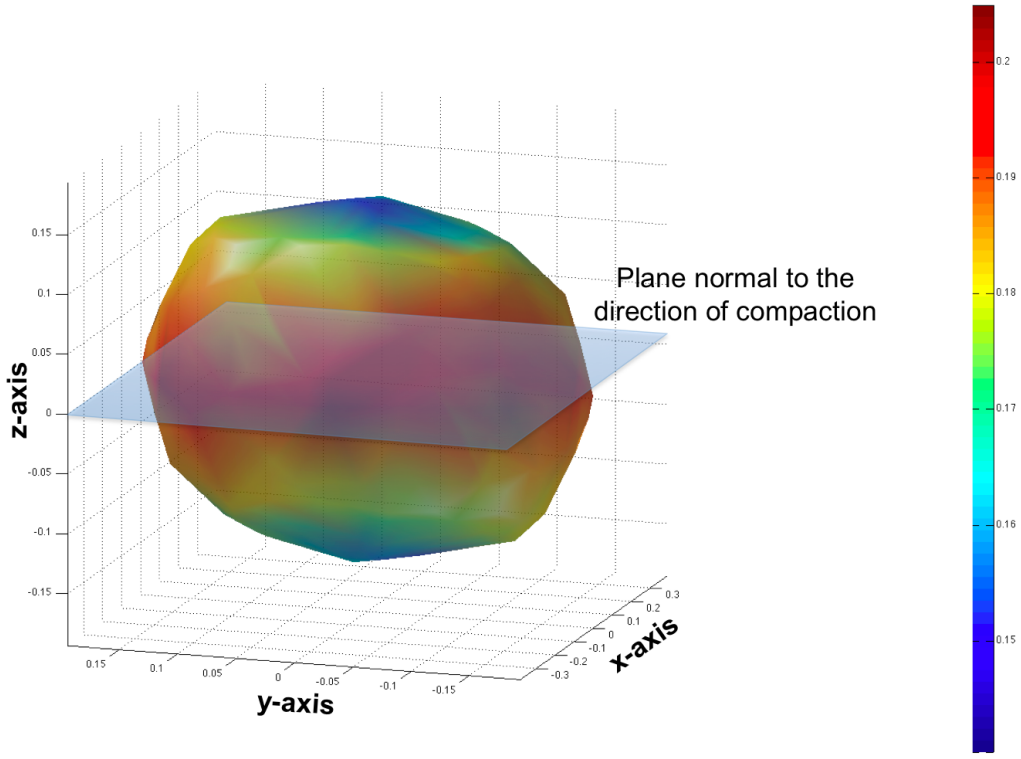

Figure 4.6. Typical Rose Diagram for the SLD with Respect to Axis of Compaction.

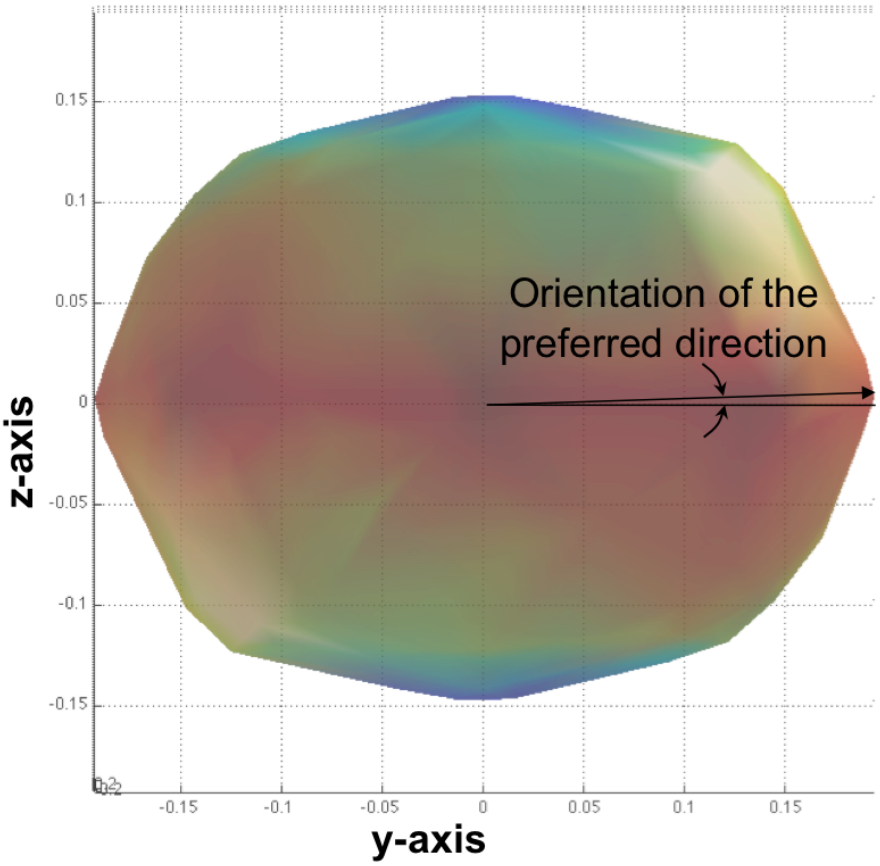

Figure 4.7. Side View Showing Orientation of the Preferred Direction.

The results based on the above metrics are summarized in Table 4.2.

Table 4.2. Summary of Results Based on Star Length Analysis of the Matrix.

Mix Type	Degree of anisotropy	Average star length in preferred direction	Average of standard deviation in star lengths	Average of coefficient of variation in star lengths	Orientation of the preferred direction (degrees)
Control Mix	1.28	0.37	0.31	103%	7.6
High Binder	1.25	0.18	0.12	84%	2.8
Fine Adjusted	1.15	0.17	0.13	83%	5.7
Coarse Adjusted	1.30	0.34	0.28	104%	45.4

Figures 4.8 and 4.9 illustrate the average SLD for the FAM specimens and the full-scale asphalt mixtures, respectively. The absolute values for the orientation of the principal direction varied mostly from 2 to 7 degrees and the results were statistically similar for all specimens and are not included here.

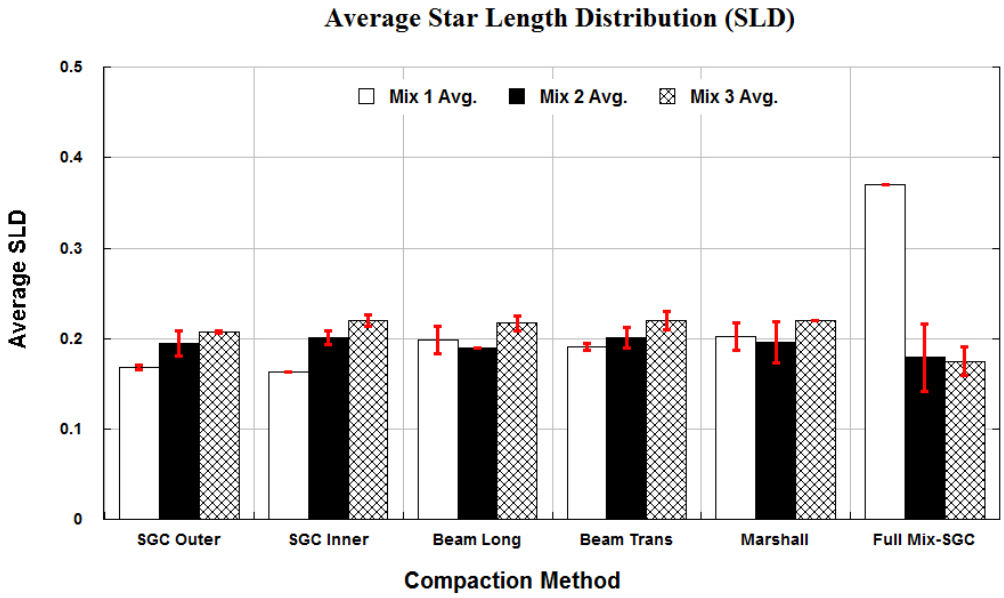

Figure 4.8. Average SLD Along Principal Direction for the FAM and Full-scale Asphalt Mixtures.

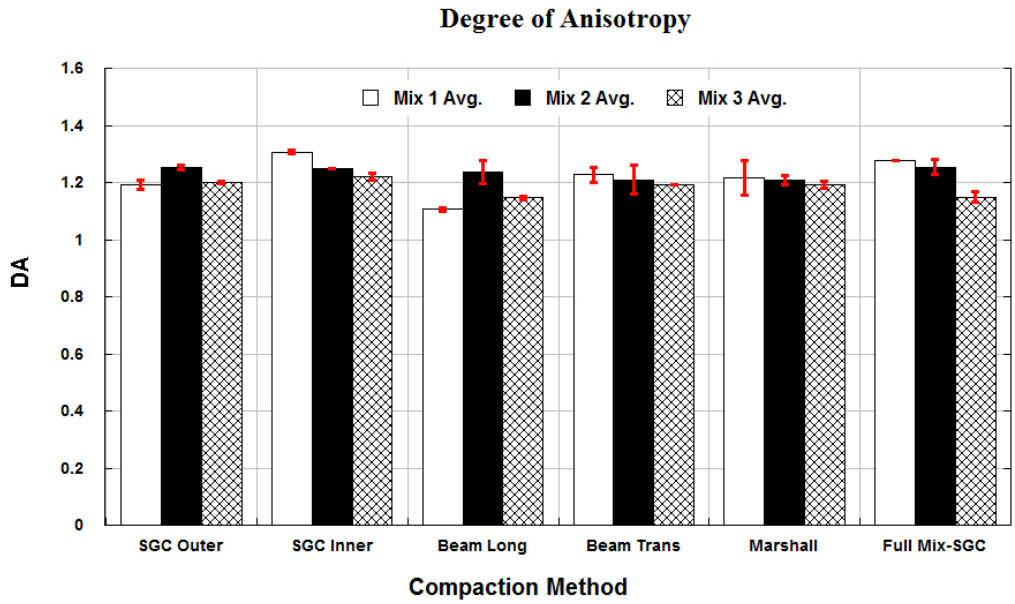

Figure 4.9. Average Degree of Anisotropy for the FAM and Full-scale Asphalt Mixtures.

Due to the limited scope of this project, only two specimens of each type were used for the X-ray tomography. Based on the results from this analysis, there appears to be some difference in the average SLD values depending on the mix type and method of compaction. However, in most cases these differences were not be significant statistically based on a t- test.

4.4 CHARACTERIZING ENGINEERING PROPERTIES

The FAM specimens were further subjected to DMA testing to evaluate the influence of mixture variables such as binder content and change in fine aggregate gradation as well the influence of the method of compaction. The DMA test was conducted by fixing one end of the FAM specimen and applying a torsional shear at the other end. Figure 4.10 illustrates the typical set up used for DMA testing.

4.4.1 Undamaged properties

The linear viscoelastic or undamaged properties of the FAM specimens were measured by applying a sinusoidal load with a constant low stress amplitude and measuring the dynamic shear modulus G^* and phase angle δ. The shear stress amplitude used was 10kPa and the frequency of loading was 5Hz. Figures 4.11 and 4.12 illustrate these two properties for the FAM specimens.

Both fine aggregate gradation and binder content had a significant influence on the mechanical properties of FAM. As expected, an increase in the asphalt binder content decreased the dynamic shear modulus and increased the phase angle of the FAM specimens. The influence of fine aggregate gradation on the dynamic shear modulus was not as significant as the asphalt binder content. Depending on the method of compaction the dynamic shear modulus and the phase angle either increased or decreased. The method of compaction had a significant influence on the dynamic shear modulus of the FAM specimens. For instance, the specimens prepared using the Marshall compaction method had the highest modulus (G^*).

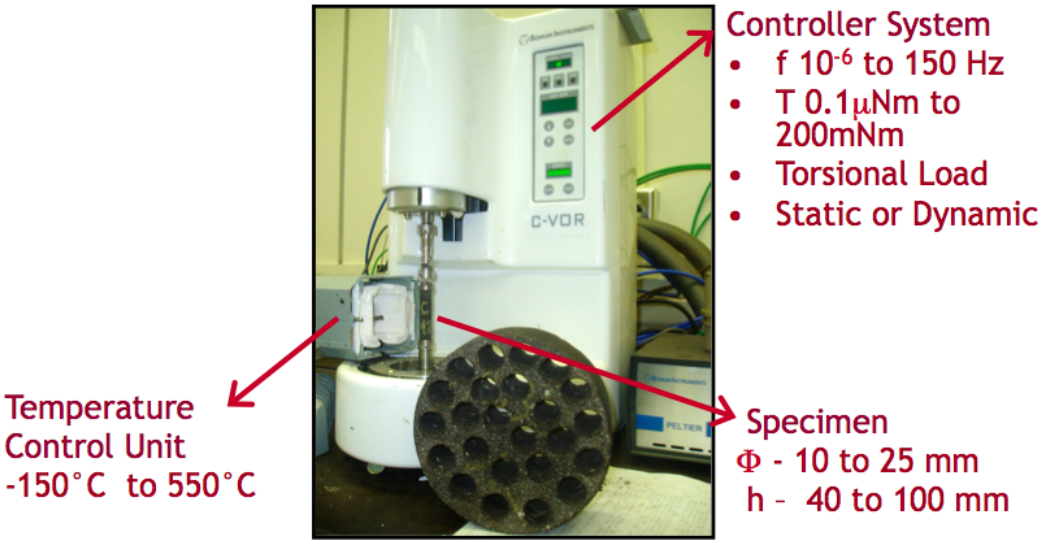

Figure 4.10. Setup of the DMA with a Typical Test Specimen.

The influence of three factors (binder content, fine aggregate gradation, and method of compaction) on the homogeneity and anisotropy of the specimen from a given method of compaction (SGC or beam) was evaluated. Comparing the two groups of specimens (inner and outer) fabricated using the Superpave Gyratory Compactor; it was observed that with a minor exception there was no significant difference in the dynamic modulus or phase angle of the specimens from the inner core compared to the specimens from the outer core. Similarly, comparing two different groups of specimens prepared using the beam compactor (Longitudinal and Transversal), the FAM specimens were mostly isotropic at these stress levels in terms of the dynamic modulus and phase angle. At higher stress levels the FAM specimens from the beam compaction demonstrated slight anisotropy. However, the degree of anisotropy was not statistically significant.

Figure 4.13 illustrates the dynamic shear modulus of the FAM specimens measured using a higher stress amplitude of 210 Kpa.

4.4.2 Fatigue crack growth

A time sweep test was conducted on the FAM specimens to characterize the fatigue cracking resistance. The time sweep was conducted by applying a sinusoidal wave form at 5Hz with a constant shear stress amplitude of 210kPa. The complex modulus of the specimen was recorded as a function of the number of load cycles. Due to the inherent variability associated with the fatigue test, the slope of the complex modulus, G^* versus $\log(time)$ was used as a characteristic for the fatigue cracking resistance of the specimen. This parameter demonstrates the lowest amount of variability between replicates in a fatigue test. Figure 4.14 illustrates the typical reduction in G^* with time and a power law fit with the relevant slope parameters. Figure 4.15 compares the rate of fatigue crack growth for the different FAM specimens.

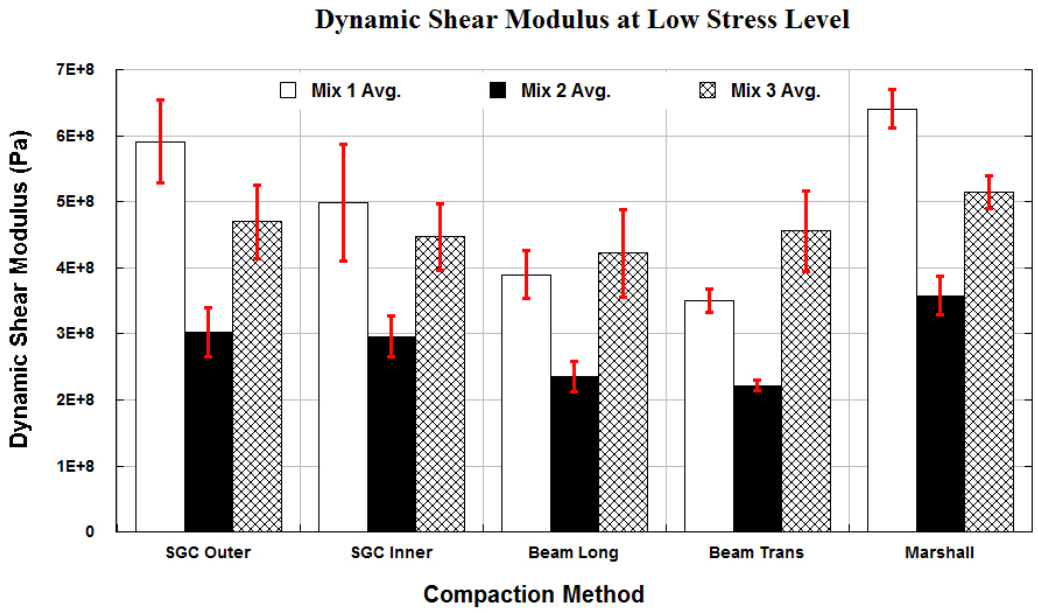

Figure 4.11. Average Linear Viscoelastic Complex Modulus for FAM Mixtures.

The results indicate that the Marshall specimens experienced the highest rate of damage growth. As expected, an increase in the binder content decreased the rate of fatigue damage. The trend in terms of the rate of damage growth for different mix types and methods of compaction was very similar to the trends observed for the complex shear modulus at the high stress level. The effect of fine aggregate gradation was not as significant as asphalt binder content. Other than the FAM specimens cored in the transverse direction from the beam compacted specimen, Mix 1 and Mix 3 demonstrated similar fatigue cracking response. Recall that Mix 1 and Mix 3 represent the control and the fine adjusted mix, respectively. The most significant difference between the fine adjusted and the control mix is the percentage of fines passing #200 sieve. Therefore, these results suggest that increasing the percentage of finer aggregates in the mix did not

significantly influence the rate of fatigue crack growth. However, since this study included only a limited number of mixtures this finding must be further investigated in future work.

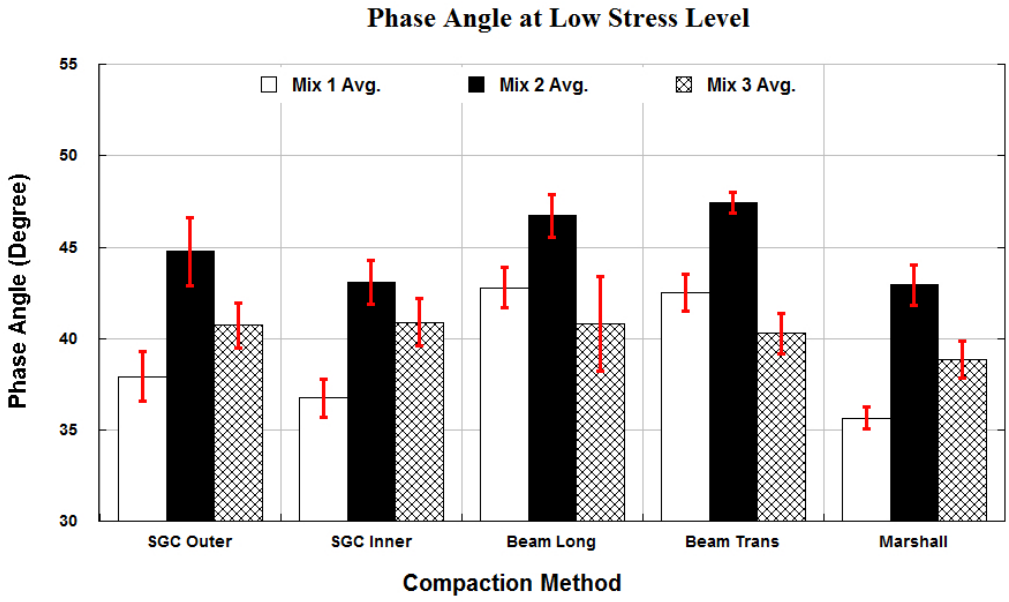

Figure 4.12. Average Linear Viscoelastic Phase Angle for FAM Mixtures.

4.4.3 Healing characteristics

The self-healing characteristics of the FAM specimens were quantified based on the following method and metrics. A time sweep test following a sinusoidal wave form in shear was conducted with a frequency of 5Hz and constant stress amplitude of 210kPa. The test was continued until the measured complex shear modulus was 50% of the linear viscoelastic complex shear modulus measured at low stress amplitudes. At this stage, the test was stopped for a duration of 30 minutes. During this rest period, the linear

viscoelastic complex shear modulus was measured by applying a shear stress following a sinusoidal wave form at a frequency of 5Hz and a stress amplitude of 10kPa for 50 cycles. This linear viscoelastic shear modulus was measured at 0.5, 1, 3, 5, 10 and 30 minutes after the start of the rest period. The increase in the linear viscoelastic shear modulus with time during the rest period was used as an indicator of the level of healing within the sample. The working assumption for this measurement was that the few load cycles applied from time to time during the rest period to measure the linear viscoelastic shear modulus will have a minimal affect on the healing process within the specimen.

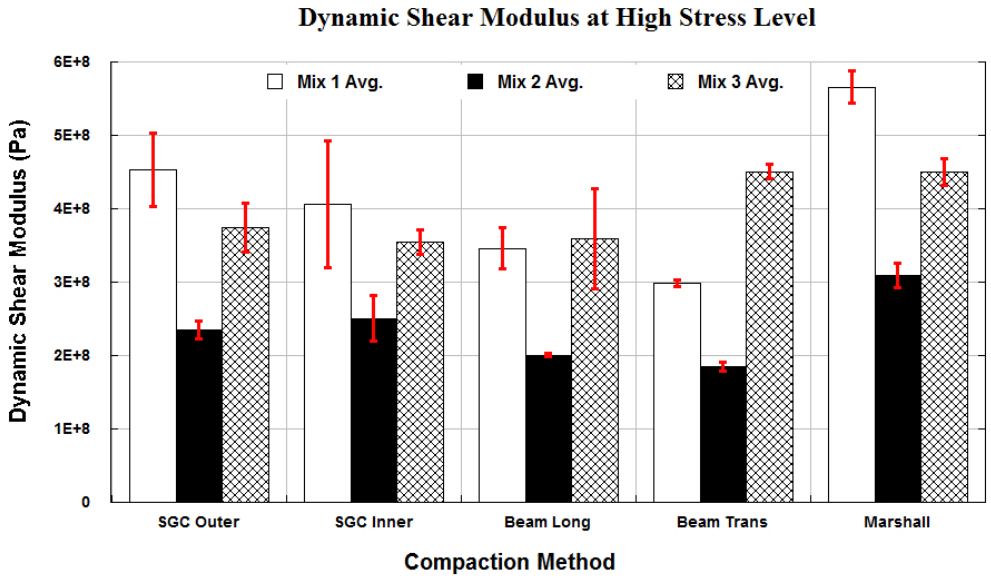

Figure 4.13. Average Viscoelastic Complex Modulus for FAM Mixtures at High Stress Levels.

After the completion of the 30-minute rest period, the complex shear modulus of the specimen had significantly increased. At this time, the application of the high amplitude

shear stress following a sinusoidal wave form with a frequency of 5Hz and stress amplitude of 210kPa was resumed. The high stress amplitude fatigue test was continued until the specimen again reached 50% of its linear viscoelastic shear stress amplitude. A second rest period of 30 minutes was introduced and the healing was recorded in terms of the linear viscoelastic complex shear modulus as before. The process was repeated for a total of four rest periods with the only exception that the fourth rest period was for 60 minutes instead of 30 minutes. After the fourth rest period the specimen was subjected to cyclic loading until failure.

The metric to quantify the healing characteristics of the FAM specimen was determined as follows. The healing or increase in the linear viscoelastic G^* during the rest period was plotted as a function of time during the rest period. This relationship was found to fit the following model:

$$\log(G^*) = c\log(t) + d \qquad (4.1)$$

where, c and d are material constants and t is time. A total of four relationships and four sets of parameters could be plotted corresponding to each one of the four rest periods. Examination of some results showed that the material parameters c and d did not change significantly from the first rest period to the fourth. Therefore, for the remainder of the work presented in this study, the parameter d from the first rest period is used as the metric that characterizes the healing properties of that specimen. Figures 4.16 and 4.17 illustrate the healing curves from the four rest periods along with the parameters indicated in equation 4.1. Figure 4.18 compares the healing characteristics for the different FAM specimens.

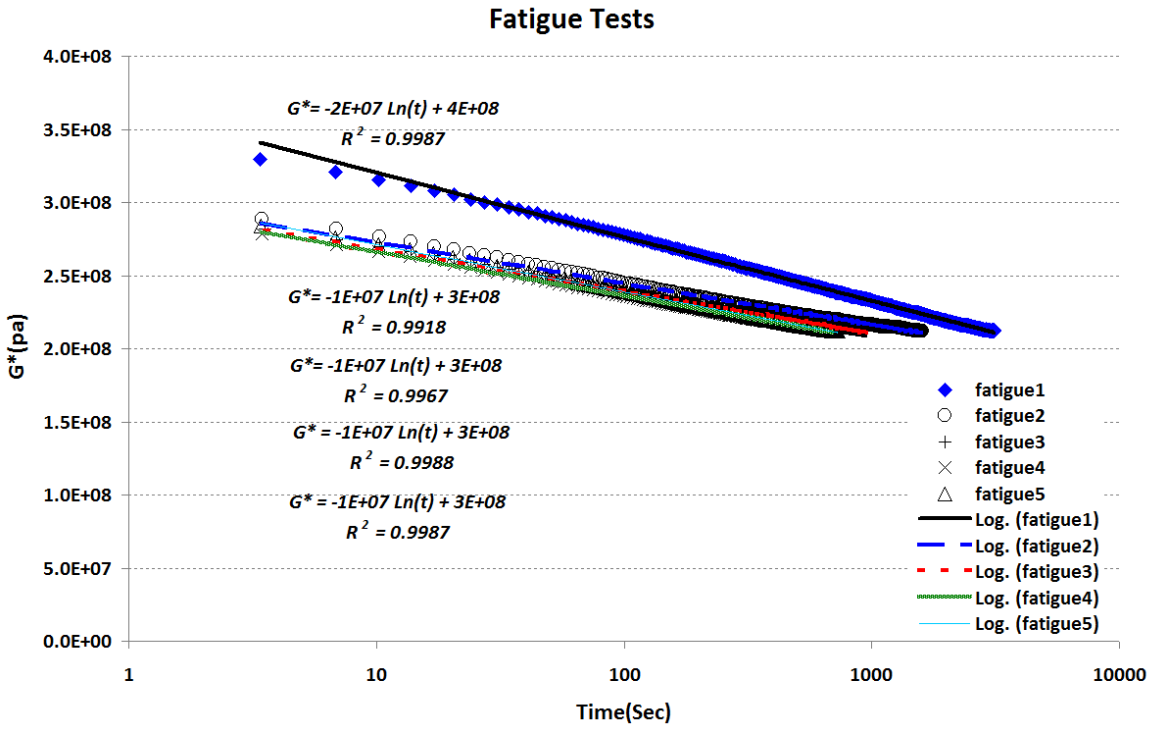

Figure 4.14. Typical Results from Fatigue Test using DMA.

Results demonstrate that an increase in the asphalt content or fines did not necessarily improve the healing characteristics of the FAM specimen. This can be explained as follows. The average dimensions of the mastic between the fine aggregate particles or average SLD has a significant influence on the fracture and healing properties of the asphalt mixture. It has been described that an increase in the binder content in asphalt mixtures did not necessarily increase the average binder volume between the fine aggregate particles. The average SLD for the full-scale mixture with high mastic volume was in fact less than the average SLD for the control mixture. Similarly, the average SLD for the FAM specimens with high mastic volume (Mix 2 and Mix 3) was not significantly different compared to the control mix, based on the number of replicates. A more

uniformly dispersed mastic with smaller average dimensions can demonstrate improved fatigue cracking resistance on account of an increased tensile strength of the binder due to higher confining pressures. Similarly, self-healing in the asphalt is strongly influenced by the crack size and volume of asphalt around the crack tip. Smaller cracks will demonstrate a higher rate of self-healing. At the same time, smaller volume of asphalt surrounding the crack (smaller average SLD dimensions) will result in reduced rate of self-healing because of an increased local stiffness surrounding the crack-tip. These mechanisms combined with the results that demonstrate that the average dimensions of the mastic distributed between the aggregate particles did not vary significantly between the three mixtures are consistent with the observation that the healing characteristics of Mixes 2 and 3 were similar to the healing characteristic of Mix 1, despite the higher percentage of the asphalt binder.

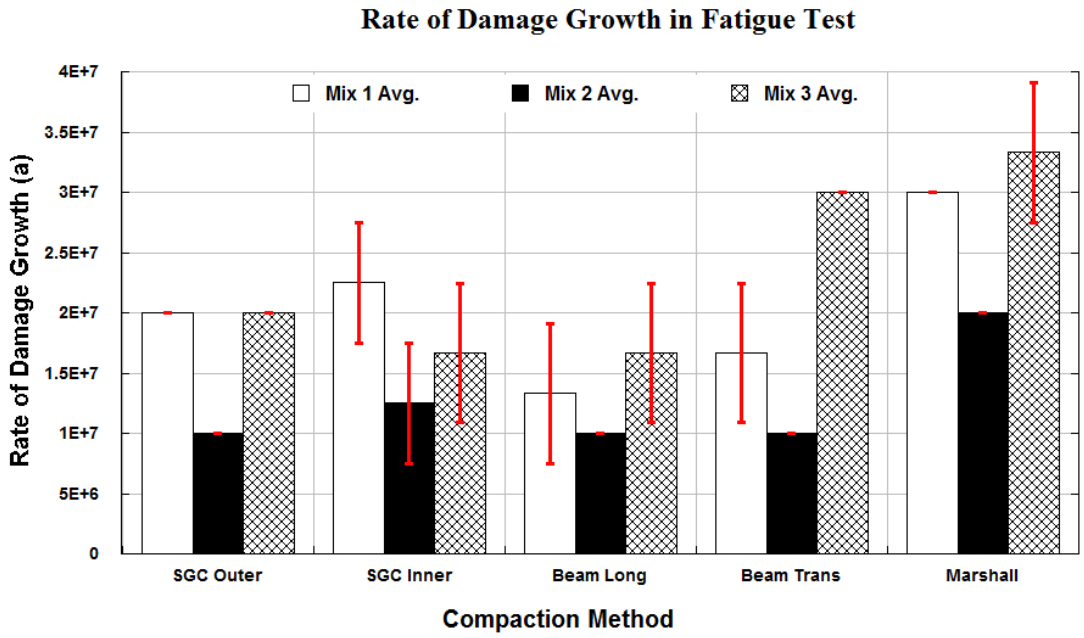

Figure 4.15. Average Fatigue Crack Growth Rate for FAM Mixtures.

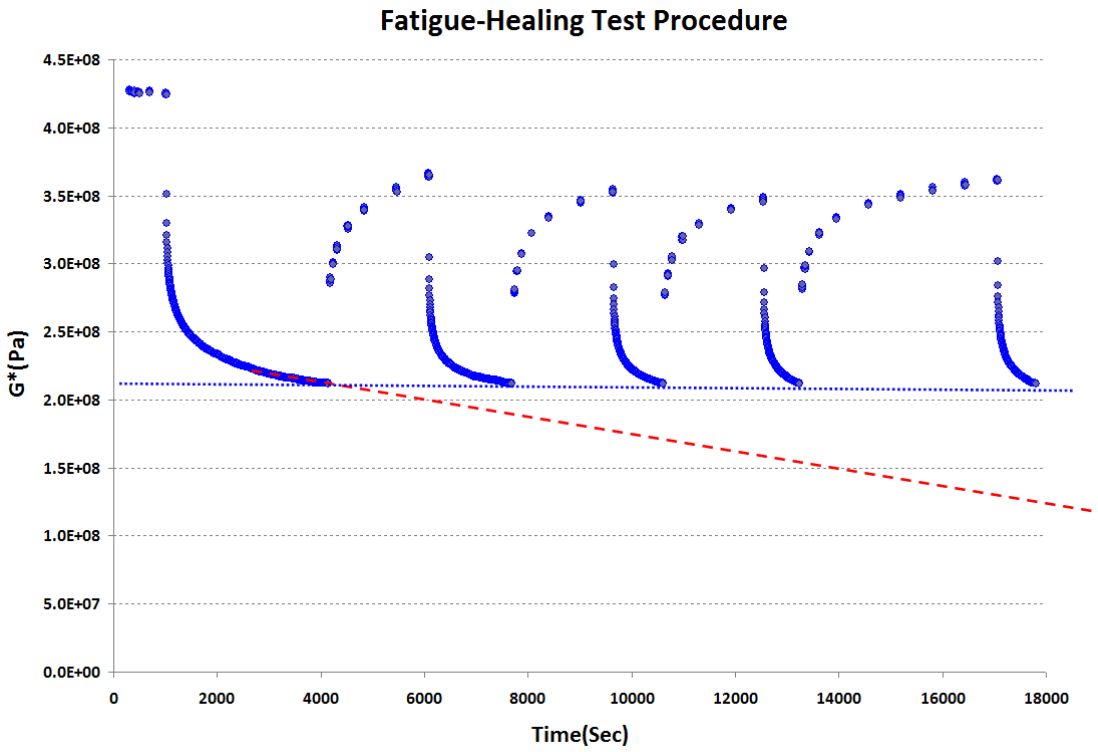

Figure 4.16. Typical Fatigue Test with Rest Periods.

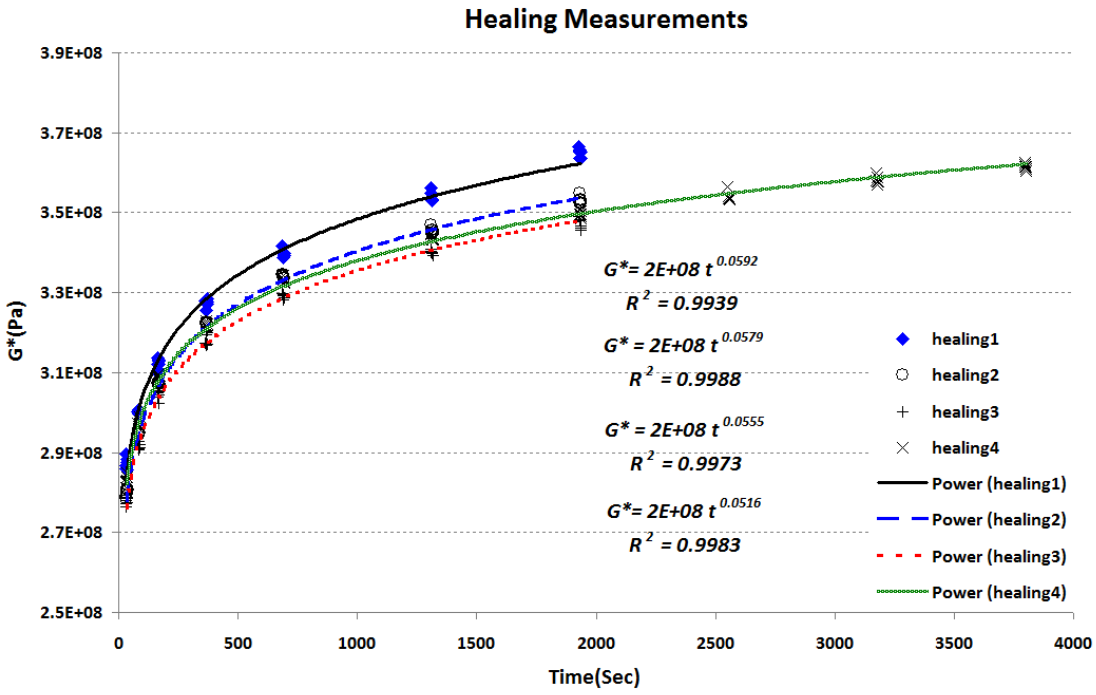

Figure 4.17. Typical Healing vs. Time Curves From Four Rest Periods.

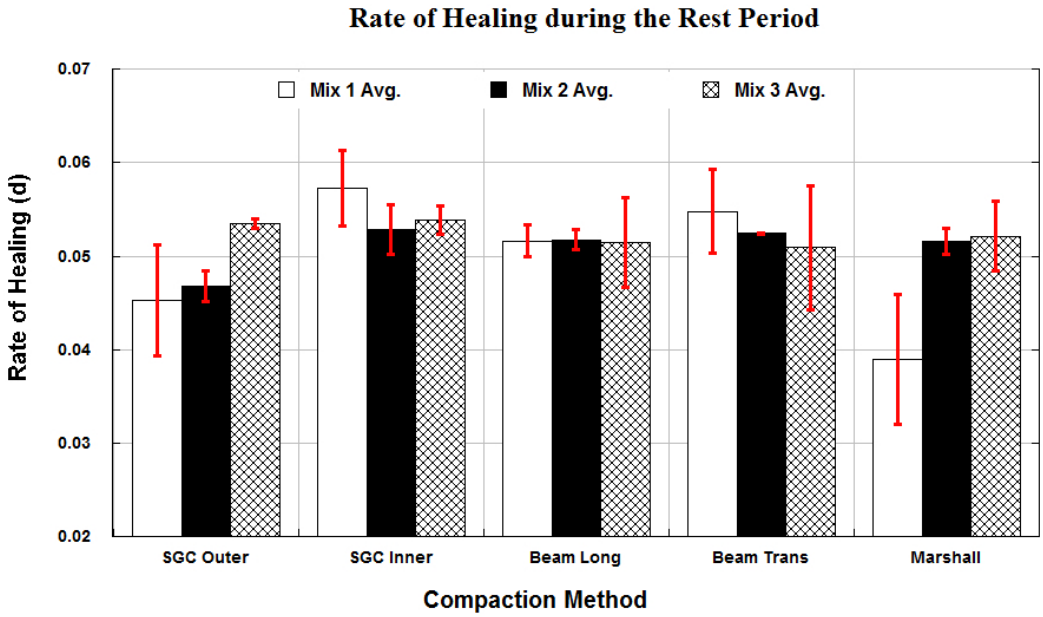

Figure 4.18. Average Healing Characteristic Parameter for FAM Mixtures.

Chapter 5. Conclusions

The first objective of this study was to establish a quantitative method to characterize the three dimensional microstructure of the asphalt binder in an asphalt mixture and to be able to relate mixture microstructure to its properties. The following are some of the conclusions that can be drawn based on the results presented in Table 4.2.

1. The asphalt binder matrix has some degree of anisotropy in all mixtures. The control and the coarse adjusted mixtures had similar and the highest level of anisotropy. This is expected, because the analysis was based on the microstructure of the asphalt matrix, which is not expected to change significantly upon changing only the coarse aggregate gradation of the mixture. Increasing the binder content, reduced the anisotropy to some extent but not significantly. Changing the gradation within the fine aggregate fraction of the mixture significantly reduced the level of anisotropy (fine adjusted mix).
2. The average star length of the asphalt mastic in the fine aggregate matrix along the preferred orientation was similar for the control and the coarse adjusted mix. This was also expected, since changes in the coarse aggregate gradation should not have a significant impact on the internal microstructure of the fine aggregate matrix. The average star length reduced significantly due to the addition of asphalt binder (high binder mix). All other variables remaining constant, contrary to the findings, one would expect that the addition of asphalt binder should increase the average star length as compared to the control mixture. This apparent contradiction can be explained as follows. The fine aggregate particles in mixtures

with higher binder content are more likely to be homogeneously distributed resulted in a more dispersed mastic-fine aggregate matrix with relative smaller average size of the asphalt mastic. This explanation is further supported by the reduced standard deviation and coefficient of variability in the star lengths for the mixtures with higher binder content. A more uniformly dispersed mastic within the matrix can have a significant influence on the mixture properties and performance. For example, a matrix where the asphalt mastic has smaller average dimensions and is more uniformly dispersed can be more effective in crack pinning and hence resisting crack growth. A change in the fine aggregate gradation also had a similar impact as the increase in binder content.

3. In most cases, the preferred direction of the asphalt mastic or direction with the largest star length was perpendicular to the direction of compaction. This indicates that the fine aggregate matrix experiences compaction induced anisotropy in addition to inherent anisotropy that may be due to the shape characteristics of the fine aggregate. For the mixture with the different coarse aggregate gradation (coarse adjusted mix), this orientation was almost 45 degrees to the direction of compaction and significantly different from other mixtures. This indicates that the coarse aggregate gradation may have an significant influence in dictating the direction of anisotropy.
4. Although all test specimens had gradations within the specification limits, they had widely different internal microstructure. The differences in the internal microstructure are expected to yield very different mechanical and damage characteristics. While the findings reported in this study are based on the use of a limited number of mixtures, the results indicate the importance of understanding

the relationship between aggregate gradation, internal microstructure, and performance.

The second objective was to compare the internal microstructure of the mortar from a full-scale asphalt mixture to the internal microstructure of a FAM specimen with a corresponding volumetric mix design. Another objective of this study was to evaluate the influence of mixture properties and methods of compaction on the engineering properties of the FAM specimens. The results from this study, although limited in number, indicate that in most cases the SGC compacted FAM specimen had a microstructure that most closely resembled the microstructure of the mortar within a full-scale asphalt mixture. Results also demonstrate that a change in the fine aggregate fraction of the aggregate did not significantly change the fatigue cracking resistance of the FAM specimens. The fatigue cracking characteristics of the FAM specimens were strongly influenced by the binder content; the percentage of fines did not have a significant influence.

The key finding from this study was that the healing characteristic of the three different types of FAM mixes was not significantly different. This is despite the fact that the percentage of fines in one of the mixes and the percentage of binder in the other mix was higher than those in the control mix. This indicates that the healing rate is mostly dictated by the type of binder and not significantly influenced by the gradation or binder content, as long as the volumetric distribution of the mastic was the same. In other words, the limited results from this study indicate that the inherent healing characteristics of the asphalt binder plays a more significant role relative to other properties (e.g. volumetrics) in the overall fatigue cracking resistance of the asphalt mixture.

Appendix. FAM design as a derivative of a full-scale mix

The following two considerations are defined prior to designing the FAM mixture:

1. The gradation of the FAM mixture basically follows the same gradation as the full-scale asphalt mixture it is designed to represent with only the portion of aggregate that pass #16 sieve.
2. The binder content by weight percent of the aggregates passing #16 sieve in the FAM mixture is the same as the binder content by weight percent of the aggregates passing #16 sieve in the full-scale asphalt mixture minus the binder absorbed by the coarse aggregate.

The following example illustrates the procedure that was used to design a typical FAM mixture as a derivative of a full-scale asphalt mixture.

A HMA mixture that will serve as the basis was first selected. An example gradation is provided in Table A.1.

Table A.1. Gradation for the full-scale asphalt mixture.

Aggregate type	Sieve size	Percent in the mix	Weight (g)	Cumulative weight (g)
Delta-Rock	3/4"–3/8"	25.4%	1,946.7	1,946.7
Centex-Rock	3/4"–3/8"	4.3%	329.6	2,276.3
Centex-Rock	3/4"–#4	17.0%	1,302.9	3,579.2
Centex-Rock	#4–#8	15.9%	1,218.6	4,797.8
Centex-Rock	#8–#16	9.5%	728.1	5,525.9
Centex-Rock	#16–#30	9.4%	720.4	6,246.3
Centex-Rock	#30–#50	6.7%	513.5	6,759.8
Centex-Rock	#50–#200	8.3%	636.1	7,395.9
Centex-Rock	Pass #200	3.5%	268.2	7,664.1
BINDER	PG 64-22	4.2%	336.0	

The following information was obtained:

- Total weight of aggregates $W_s = 7664.1g$
- Aggregate gradation (% passing vs. sieve size): as shown in Table A.1
- Percentage of binder $P_b = 4.2\%$
- Maximum specific gravity of a mix, G_{mm-R16}, using only aggregates retained on #16 sieve and any known amount of binder that is sufficient to completely coat the aggregate particles, P_{b-R16}. In this example G_{mm} was measured to be 2.442 and P_{b-R16} was 4.8%.
- The bulk specific gravity, G_{sb-R16}, of aggregates retained on #16 sieve i.e. 2.54 for this example.
- The specific gravity of the binder, G_b, i.e. 1.03 for this example.
- The G_{se-R16} of aggregates retained on #16 was calculated using the following equation:

$$G_{se-R16} = \frac{100 - P_{b-R16}}{\frac{100}{G_{mm-R16}} - \frac{P_{b-R16}}{G_b}} \quad \text{(A.1)}$$

- The percent weight of binder absorbed into aggregates retained on #16 was calculated using the following equation:

$$P_{ba-R16} = \frac{(100 * G_b)(G_{se-R16} - G_{sb-R16})}{(G_{se} * G_{sb-R16})} \quad \text{(A.2)}$$

- Weight of the binder absorbed in the coarse aggregate fraction is computed as:

$$W_{ba-R16} = P_{ba-R16} * \text{Weight of aggregates retained on \#16} \quad \text{(A.3)}$$

- Finally, weight of the binder in the FAM is determined as:

$$W_{b-FAM} = W_b - W_{b-R16} \quad \text{(A.4)}$$

- The Table below lists the final mix design for this FAM mix.

Table A.2. Mix design for the FAM.

Aggregate type	Sieve size	Percent in the mix	Weight (g)	Cumulative weight (g)
Centex-Rock	#16–#30	30.0%	720.4	720.4
Centex-Rock	#30–#50	21.4%	513.5	1,233.9
Centex-Rock	#50–#200	26.5%	636.1	1,870.0
Centex-Rock	Pass #200	11.2%	268.2	2,138.2
BINDER	PG 64-22	11.0%	265.3	2,403.5

Bibliography

Arambula, E., Masad, E., Martin, A.E., 2007. Influence of Air Void Distribution on the Moisture Susceptibility of Asphalt Mixes. Journal of Materials in Civil Engineering 19, 655–664.

Bhasin, A., Badgekar, S., Izadi, A., 2009. Quantitative Characterization of Asphalt Mixtures (Final Report No. 476660-00070-1). Southwest Region University Transportation Center.

Bhasin, A., Little, D.N., Bommavaram, R., Vasconcelos, K.L., 2008. A Framework to Quantify the Effect of Healing in Bituminous Materials Using Material Properties. International Journal of Road Materials and Pavement Design 9, 219–242.

Branco, V.C., Masad, E., Bhasin, A., Little, D.N., 2008. Fatigue Analysis of Asphalt Mixtures Independent of Mode of Loading. Transportation Research Record 2057, 149–156.

Brinson, H.F., Brinson, L.C., 2008. Polymer Engineering Science and Viscoelasticity. Springer.

Caro, S., Masad, E., Airey, G.D., Bhasin, A., Little, D.N., 2008. Probabilistic Analysis of Fracture in Asphalt Mixtures Caused by Moisture Damage. Transportation Research Record 2057, 28–36.

Carpenter, S.H., Shen, S., 2006. A Dissipated Energy Approach to Study HMA Healing in Fatigue, in: 85th Annual Meeting of the Transportation Research Board. Washington D.C.

Cherepanov, G.P., 1968. Cracks in solids. International Journal of Solids and Structures 4, 811 – 831.

Cowin, S.C., 1985. The relationship between the elasticity tensor and the fabric tensor. Mechanics of Materials 4, 137 – 147.

Crochet, M.J., 1966. Symmetric deformations of viscoelastic-plastic cylinders. Journal of Applied Mechanics 33, 327.

Duxson, P., Provis, J.L., Lukey, G.C., Mallicoat, S.W., Kriven, W.M., Deventer, J.S.J. van, 2005. Understanding the relationship between geopolymer composition, microstructure and mechanical properties. Colloids and Surfaces A: Physicochemical and Engineering Aspects 269, 47 – 58.

Elseifi, M., Al-Qadi, I., Yang, S.-H., Carpenter, S., 2008. Validity of Asphalt Binder Film Thickness Concept in Hot-Mix Asphalt. Transportation Research Record: Journal of the Transportation Research Board 2057, 37–45.

Ferry, J.D., 1961. Viscoelastic Properties of Polymers. John Wiley & Sons, New York.

Harrigan, T.P., Mann, R.W., 1984. Characterization of Microstructural Anitsotropy in Orthotropic Materials Using a Second Rank Tensor. Journal of Materials Science 19, 761–767.

Huang, C.-W., Masad, E., Muliana, A., Bahia, H., 2007. Nonlinearly viscoelastic analysis of asphalt mixes subjected to shear loading. Mechanics of Time-Dependent Materials 11, 91–110.

Hunter, A., Airey, G., Collop, A., 2004. Aggregate Orientation and Segregation in Laboratory-Compacted Asphalt Samples. Transportation Research Record: Journal of the Transportation Research Board 1891, 8–15.

Ketcham, R.A., 2005a. Three-dimensional Grain Fabric Measurements Using High-Resolution X-Ray Computed Tomography. Journal of Structural Geology 27, 1217–1228.

Ketcham, R.A., 2005b. Computational Methods for Quantitative Analysis of Three-dimensional Features in Geological Specimens. Geosphere 1, 32–41.

Ketcham, R.A., Carlson, W.D., 2001. Acquisition, optimization and interpretation of X-ray computed tomographic imagery: Applications to the geosciences. Computers & Geosciences 27, 381–400.

Kim, B., Roque, R., 2006. Evaluation of Healing Property of Asphalt Mixture, in: 85th Annual Meeting of the Transportation Research Board. Washington, D.C.

Kim, Y., Little, D.N., 2005. Development of Specification Type Tests to Assess the Impact of Fine Aggregate and Mineral Filler on Fatigue Damage (No. 0-1707-10). Texas Transportaion Institute.

Kim, Y.R., Little, D.N., Lytton, R.L., 2004. Effect of Moisture Damage on Material Properties and Fatigue Resistance of Asphalt Mixtures. Transportation Research Record: Journal of the Transportation Research Board 1891, 48–54.

Kim, Y.R., Little, D.N., Song, I., 2003. Effect of Mineral FIllers on Fatigue Resistance and Fundamental Material Characteristics: Mechanistic Evaluation. Transportation Research Record: Journal of the Transportation Research Board 1832, 1–8.

Lakes, R., 2009. Viscoelastic Materials. Cambridge University Press.

Little, D.N., Lytton, R.L., Williams, A.D., Chen, C.W., 2001. Microdamage Healing in Asphalt and Asphalt Concrete, Volume I: Microdamage and Microdamage Healing, Project Summary Report (No. FHWA-RD-98-141). Texas Transportation Institution, College Station, TX.

Maillard, S., de La Roche, C., Hammoum, F., Gaillet, L., Such, C., 2004. Experimental Investigation of Fracture and Healing at Pseudo-Contact of Two Aggregates, in: 3rd Euroasphalt and Eurobitume Congress. Vienna.

Masad, E., Branco, V.C., Little, D.N., 2006. Fatigue Damage: Analysis of Mastic Fatigue Damage Using Stress Controlled and Strain Controlled Test (No. 473630). Texas Transportation Institute in cooperation with Federal Highway Administration and Western Research Institute.

Masad, E., Button, J., 2004. Implications of Experimental Measurements and Analyses of the Internal Structure of Hot-Mix Asphalt. Transportation Research Record: Journal of the Transportation Research Board 1891, 212–220.

Masad, E., Huang, C.-W., Airey, G., Muliana, A., 2008. Nonlinear viscoelastic analysis of unaged and aged asphalt binders. Construction and Building Materials 22, 2170–2179.

Masad, E., Muhunthan, B., Shashidhar, N., Harman, T., 1999a. Internal Structure Characterization of Asphalt Concrete Using Image Analysis. Journal of Computing in Civil Engineering 13, 88–95.

Masad, E., Muhunthan, B., Shashidhar, N., Harman, T., 1999b. Quantifying Laboratory Compaction Effects on the Internal Structure of Asphalt Concrete. Transportation Research Record: Journal of the Transportation Research Board 1681, 179–185.

Masad, E., Tashman, L., Somedavan, N., Little, D., 2002. Micromechanics-Based Analysis of Stiffness Anisotropy in Asphalt Mixtures. Journal of Materials in Civil Engineering 14, 374–383.

Odgaard, A., 1997. Three-dimensional methods for quantification of cancellous bone architecture. Bone 20, 315 – 328.

Rice, J.R., 1968. A Path Independent Integral and the Approximate Analysis of Strain Concentration by Notches and Cracks. Journal of Applied Mechanics 35, 379–386.

Russ, J., 2007. The image processing handbook, 5th ed. ed. CRC/Taylor and Francis, Boca Raton.

Ryan, T.M., Ketcham, R.A., 2002. The three-dimensional structure of trabecular bone in the femoral head of strepsirrhine primates. Journal of Human Evolution 43, 1 – 26.

Schapery, R.A., 1975a. A Theory of Crack Initiation and Growth in Viscoelastic Media, I. Theoretical Development. International Journal of Fracture 11, 141–159.

Schapery, R.A., 1975b. A Theory of Crack Initiation and Growth in Viscoelastic Media, II. Approximate Methods of Analysis. International Journal of Fracture 11, 369–388.

Schapery, R.A., 1975c. A Theory of Crack Initiation and Growth in Viscoelastic Media, III. Analysis of Continuous Growth. International Journal of Fracture 11, 549–562.

Schapery, R.A., 1984. Correspondence Principles and a Generalized J Integral for Large Deformation and Fracture Analysis of Viscoelastic Media. International Journal of Fracture 25, 195–223.

Tashman, L., Masad, E., Little, D., Zbib, H., 2005. A microstructure-based viscoplastic model for asphalt concrete. International Journal of Plasticity 21, 1659–1685.

Torquoato, S., Lu, B., 1993. Chord-length Distribution Function for Two-phase Ramdom Media. Physical Review E 47, 2950–2954.

Tutumluer, E., Huang, H., Hashash, Y.M.A., Ghaboussi, J., 2008. Imaging Based Discrete Element Modeling of Granular Assemblies. AIP Conference Proceedings 973, 544–549.

Wang, L., Frost, J., Shashidhar, N., 2001. Microstructure Study of WesTrack Mixes from X-Ray Tomography Images. Transportation Research Record: Journal of the Transportation Research Board 1767, 85–94.

Wang, L., Park, J.-Y., Fu, Y., 2007. Representation of real particles for DEM simulation using X-ray tomography. Construction and Building Materials 21, 338–346.

Watson, G.S., 1966. The Statistics of Orientation Data. The Journal of Geology 74, 786–797.

Wineman, A.S., Rajagopal, K.R., 2000. Mechanical Response of Polymers: An Introduction. Cambridge University Press, Cambridge.

You, Z., Adhikari, S., Emin Kutay, M., 2009. Dynamic modulus simulation of the asphalt concrete using the X-ray computed tomography images. Materials and Structures 42, 617–630.

Yue, Z.Q., Bekking, W., Morin, I., 1995. Application of digital image processing to quantitative study of asphalt concrete microstructure. Transportation Research Record 1492, 53–60.

Zelelew, H., Papagiannakis, A.T., Masad, E., 2008. Application of digital image processing techniques for asphalt concrete mixture images, in: The 12th International Conference of IACMAG. Goa, India, pp. 119–124.

Zollinger, C., 2005. Application of Surface Energy Measurements to Evaluate Moisture Susceptibility of Asphalt and Aggregates.